THE TIME-DEPENDANT CRACKING BEHAVIOUR OF STRAIN HARDENING CEMENT-BASED COMPOSITE

By

Christo Johan Adendorff

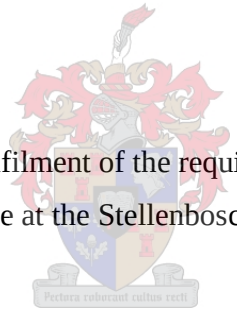

Thesis presented in partial fulfilment of the requirements for the degree of Master of Science at the Stellenbosch University

Supervisor:

Dr. W.P. Boshoff

DECEMBER 2009

DECLARATION

By submitting this thesis electronically, I declare that the entirety of the work contained therein is my own, original work, that I am the owner of the copyright thereof (unless to the extent explicitly otherwise stated) and that I have not previously in its entirety or in part submitted it for obtaining any qualification.

Date: December 2009

Signature: _____

SUMMARY

Strain Hardening Cement-based Composite (SHCC) is part of the High Performance Fibre Reinforced Cement-based Composite (HPFRCC) family and is a relative new concrete composite. This Fibre Reinforced Cement-based Composite (FRCC) contains randomly distributed short fibres and when subjected to a uni-axial tensile load multiple cracking occurs. The multiple cracking generates fine cracks which are normally smaller than 100 µm and achieve a strain capacity of more than 5 %. There are limited publications regarding the research of sustained tensile tests on SHCC and especially the cracking behaviour of SHCC under quasi-static uni-axial as well as sustained tensile loads.

The cracking behaviour is described as the average crack width, number of cracks and descriptive statistical properties which could be used to represent the distribution of the multiple fine cracks under uni-axial tension. There are two types of tests that were under consideration to determine the cracking behaviour of SHCC. The first is quasi-static uni-axial tensile tests and the second is sustained tensile tests. The latter was dependant on the uni-axial tensile tests in terms of the sustained load applied. The sustained loads ranged from 40 % to 80 % of the ultimate tensile resistance recorded from the uni-axial tensile tests that correspond with a strain rate of 0.001 /s. Different strain rates were used for the uni-axial tensile tests to determine the effect on the cracking behaviour. The cracking behaviour was determined with the aid of a non-contact optical 3D digital deformation measuring device called ARAMIS.

The content of this thesis gives a background study of the cracking behaviour and relevant research performed on SHCC under certain loads as well as some literature about the time-dependant effects of a cement-based composite.

The functioning of the device called ARAMIS is explained as well as the resulting effects of this device on the preparation of the test specimens. The experimental framework for the uni-axial and sustained tensile tests is discussed.

Thereafter, the experimental results of the tests are depicted and discussed. The results shed some light on the basic material properties such as the average ultimate stress and average ultimate strain, Young's modulus, etc. for the quasi-static tensile tests as well as shrinkage and creep of SHCC. The cracking behaviour such as the average crack width, number of cracks, the variance and skewness of the distribution of the crack widths in the test specimens for the quasi-static uni-axial and sustained tensile tests are depicted and discussed.

The cracking behaviour when subjected to uni-axial tensile tests with different strain rates is significantly governed by the formation of new cracks and the average crack width remains small with increase in strain. There is no significant difference for the cracking behaviour found when subjected to different strain rates. However, when SHCC is subjected to a sustained load then the average crack width is dependant on the number of cracks that form over time as well as the load level. The formation of fewer and wider cracks was observed for specimens loaded at average 40 % of the ultimate tensile resistance stress, however at loading percentages of higher than 65 % more cracks developed which resulted in a smaller average crack width.

OPSOMMING

Vervorming Verharding Sement gebaseerde samestelling “Strain Hardening Cement-based Composite” (SHCC) is deel van die familie van “High Performance Fibre Reinforced Cement-based Composite” (HPFRCC) en is ’n relatiewe nuwe beton samestelling. Hierdie vesel versterkte sement gebaseerde beton bevat willekeurig verspreide kort vesels en veelvoudige klein krake vorm onder monotoniese trekkragte. Hierdie veelvoudige klein krake is minder as 100 µm wyd en lei tot ’n vervorming van meer as 5 %. Daar is ’n tekort aan navorsing oor die kruip van SHCC sowel as die kraak gedrag van hierdie sement gebaseerde samestelling onderhewig aan trek.

Die kraak gedrag word beskryf as die gemiddelde kraakwydte, aantal krake en ’n paar beskrywende statistiese parameters. Hierdie kraak gedrag parameters kan gebruik word om ’n verdeling te kan weergee van die veelvoudige klein krake onder ’n trek belasting. Twee tipes toetse was uitgevoer om die kraak gedrag te beskryf. Die eerste tipe toets was monotoniese trek toetse en die tweede tipe was kruip toetse. Die tweede toets was afhanklik van die monotoniese trek toetse in terme van die belasting wat gebruik was vir die kruip toetse. Die belasting was gevarieer vanaf 40 % tot 80 % van die breekbelasting wat bepaal is met die monotoniese trektoetse wat ooreenstem met ’n vervorming tempo van 0.001 /s. Verskillende vervorming tempo’s vir die monotoniese trektoetse was uitgevoer om te bepaal wat die effek is op die kraak gedrag. Die kraak gedrag was bepaal met behulp van ’n geen-kontak optiese 3D digitale deformasie meet instrument genoem ARAMIS.

Die inhoud van die tesis bevat ’n kort opsoming oor ’n agtergrond studie van die kraak gedrag en relevante navorsing oor vesel versterkte sement gebaseerde beton, sowel as literatuur oor die tydafhanklike effekte van ’n sement gebaseerde samestelling.

Die beheer en gebruik van die meet instrument ARAMIS word verduidelik, sowel as die effek van hierdie masjien op die voorbereiding vir die eksperimente. Die eksperimentele uiteensetting vir die monotoniese en kruip toetse word beskryf.

Daarvolgens is die resultate van die eksperimentele toetse getoon en verduidelik. Die resultate verduidelik die basiese materiaal eienskappe, byvoorbeeld die gemiddelde breekspanning met die ooreenkomstige breekvervorming, Young's modulus en so voorts vir die monotoniese trektoetse, sowel as eienskappe met betrekking tot krimp en kruip van SHCC. Die kraak gedrag naamlik die gemiddelde kraakwydte, aantal krake per meter, variansie en die skuinsheid van die ontwikkelde krake met die toets proefstukke vir die monotoniese en kruip trek toetse word weergegee en verduidelik.

Die kraak gedrag van SHCC wanneer getoets word met verskillende monotoniese trektoets tempo's word beheer deur die ontwikkeling van nuwe krake en die gemiddelde kraakwydte is beduidend laag met toenemende vervorming. Daar is geen beduidende verskil in die kraak gedrag ten opsigte van die verskillende monotoniese trek tempo's nie. In teendeel, wanneer SHCC belas word met 'n konstante las oor tyd word die gemiddelde kraakwydte beheer deur die ontwikkeling van nuwe krake sowel as die belasting wat aangewend is. Onder 'n belasting van so laag as 40 % van die breekbelasting vorm daar minder krake, maar met 'n groter gemiddelde kraakwydte. Wanneer belas word met meer as 65 % van die breekbelasting vorm meer krake wat lei tot 'n kleiner gemiddelde kraakwydte.

ACKNOWLEDGMENTS

I would like to thank Doctor Billy Boshoff my study leader. His guidance and great knowledge contributed enormously to my understanding of concepts and the identification of problems as well as problem-solving.

I would like to thank My Parents and my sister for their continuous support throughout my life.

I would like to thank Professor G.P.A.G. van Zijl for his support and insight and great knowledge.

I would like to express my gratitude to Mr. Charlton Ramat, Mr. Arthur Layman, Mr. Godwin Groenewald as well as Mr. Coenie Enslin and Mr. Adriaan Fouche for their time and effort in assisting with the experimental work in the laboratories.

I would like to express my gratitude to Mr. Dion Viljoen and Mr. Johan van der Merwe from the workshop. They are very innovative and practical.

LIST OF TABLES

Table 1. SHCC constituents.....6

Table 2. SHCC constituents, ratio's and mix proportions.....23

Table 3. The number of specimens used for each loading rate test.....36

Table 4. The loading percentage and duration for each sustained tensile test.....41

Table 5. The E-modulus for the 0.001 /s strain rate.....46

Table 6. Crack width determined with the ARAMIS system and the CAD software.....61

LIST OF FIGURES

Figure 1. A stress-strain graph illustrating the strain-hardening of SHCC under tensile loading 4

Figure 2. The fibre, matrix and interfacial properties.....7

Figure 3. The σ-δ curve and the concept of complementary energy (area labelled C),.....7

Figure 4. Energy performance indices (Li et al., 2001).....9

Figure 5. (a) Single fibre normal pull-out; (b) Inclined fibre pull-out (Li, 1993) 10

Figure 6. Tensile response of a pseudo strain-hardening FRCC (Li, 1992) 15

Figure 7. Phase representation of creep over time for ordinary concrete 17

Figure 8. Load-deflection response showing the failure of four sustained loads at 92%, 85%, 80%, and 76% of the ultimate resistance load (Zhou, 1992).....18

Figure 9. The non-linear behaviour of creep relative to the applied load ratio 18

Figure 10. Aggregate grading: Local silica sand type Console number 2 22

Figure 11. The flow table used for the testing of the rheology.....24

Figure 12. A steel mould and lid for the test specimens with the two removable studs.....25

Figure 13. Dimensions of the test specimens 26

Figure 14. a) The temperature in the climate room and b) The relative humidity of the climate room 27

Figure 15. Specimen with painted layer of limestone 27

Figure 16. Enlarged view of the stochastic pattern on the specimen.....28

Figure 17. A masked area on a stage that was analysed.....29

Figure 18. Facet sizes of 15 x 15 with a 2 pixel overlap (ARAMIS help file).....29

Figure 19. Position of section line on the analysed area.....30

Figure 20. Idealisation of a crack growth for a specimen undergoing a uni-axial tensile load 31

Figure 21. a) The developed cracks for a specimen at a specific strain b) The analysed area showing the physical cracks with contours with the aid of the ARAMIS software 32

Figure 22. The two LVDTs connected to a frame and connected to the specimen 34

Figure 23. The clamps used for the uni-axial tensile tests in the Zwick.....35

Figure 24. Sustained tensile loading setup.....37

Figure 25. Schematic representation of the sustained tensile loading setup.....37

Figure 26. The clamps used for the sustained tensile tests a) front view and b) side view ..39

Figure 27. Setup of the shrinkage specimens 39

Figure 28. Stress-strain responses for each loading rate from the lowest to the highest strain rate 44

Figure 29. Average ultimate tensile stress and average ultimate tensile strain with the minimum and maximum values indicated for each strain rate 45

Figure 30. Representation of the non-linear initial ascending branch (Boshoff, 2007).....46

Figure 31. The shrinkage strain readings for the four test specimens 48

Figure 32. Averaged shrinkage strains for the three specimens 48

Figure 33. The creep results of the specimens not used for the crack analysis 49

Figure 34. The creep strains for the twelve specimens that were used to determine the cracking behaviour, with loading percentages varying between 40 % and 80 %.....50

Figure 35. The creep compliance for each load ratio at different time frames.....51

Figure 36. The time to fracture for all the creep specimens 52

Figure 37. a) A distribution skewed right and b) a distribution skewed left 57

Figure 38. The displacement determined with the shown x and y coordinates system.....59

Figure 39. Typical crack pattern observed for a creep test specimen at 1.7 days, 2.7 days and 6.9 days 60

Figure 40. a) The test specimen shown with the developed cracks and the maximum crack that was measured in the CAD software, b) Enlarged view of the measured crack, c) Even more enlarged view of crack.....62

Figure 41. The chosen strain values with the corresponding stress values for the different strain rates 64

Figure 42. The average crack width for each test specimen for each strain rate 65

Figure 43. The variance of the crack width distribution for each test specimen for each strain rate.....66

Figure 44. The number of cracks for each test specimen for each strain rate 67

Figure 45. The skewness of the crack width distribution for each test specimen for each strain rate.....68

Figure 46. The average of the cracking behaviour characteristics for the different loading rates 69

Figure 47. The average crack width and number of cracks per meter for selected strains...69

Figure 48. The average crack width for the ten specimens 71

Figure 49. The variance of the crack width distribution for the ten specimens.....72

Figure 50. The number of cracks for the ten specimens.....73

Figure 51. The skewness of the distribution of the crack widths for the ten specimens 74

Figure 52. Comparison of the two types of tensile tests with regard to the cracking behaviour characteristics.....77

TABLE OF CONTENTS

DECLARATION .....

SUMMARY i

OPSOMMING iii

ACKNOWLEDGMENTS v

LIST OF TABLES vi

LIST OF FIGURES vii

TABLE OF CONTENTS xi

CHAPTER 1 1

INTRODUCTION 1

1.1 Background 1

1.2 Aim and Scope 2

1.3 Outline of Contents 3

CHAPTER 2 4

BACKGROUND STUDY 4

2.1 Background of SHCC 4

2.2 SHCC Constituents and Fibre Behaviour 5

2.3 Cracking Behaviour 11

2.4 Time-Dependant Effects: Creep and Shrinkage 16

2.5 Summary 19

CHAPTER 3 21

EXPERIMENTAL FRAMEWORK 21

3.1 Introduction 21

3.2 Specimen Preparation 21

3.3 Digital Deformation Measurement System 28

3.4 Uni-axial Quasi-static Tensile Tests 33

3.4.1 Research program 33

3.4.2 Experimental methodology and setup 33

3.4.3 Experimental program 35

3.5 Sustained Tensile Loading and Shrinkage Tests 36

3.5.1 Research program 36

3.5.2 Experimental methodology and setup 36

3.5.3 Experimental program 40

3.6 Summary 41

CHAPTER 4 43

TESTS RESULTS 43

4.1 Introduction 43

4.2 Uni-axial Quasi-static Tensile Tests 43

4.2.1 Basic material properties 43

4.3 Shrinkage and Sustained Tensile Loading Tests 47

4.3.1 Shrinkage 47

4.3.2 Creep 49

4.4 Discussion 52

4.5 Summary 54

CHAPTER 5 55

CRACKING BEHAVIOUR 55

5.1 Introduction 55

5.2 Crack Pattern Analysis Framework 56

5.3 Quasi-static Cracking Behaviour 63

5.4 Sustained Loading Cracking Behaviour 70

5.5 Discussion 74

5.6 Summary 78

CHAPTER 6 79

CONCLUSIONS AND FUTURE DEVELOPMENTS 79

6.1 Conclusions 79

6.2 Future Developments 81

CHAPTER 7 83

REFERENCES 83

CHAPTER 1

INTRODUCTION

1.1 Background

The increasing growth of advanced technology promotes the capability to investigate new advanced materials and composites and their behaviour under specific conditions. Strain Hardening Cement-based Composite (SHCC) is part of the High Performance Fibre Reinforced Cement-based Composite (HPFRCC) family and is a relative new concrete composite. SHCC contain randomly distributed short fibres and gives rise to multiple cracking under uni-axial tensile loading as well as in bending (Boshoff, 2007). This cement-based composite can be used where high tensile strains occur and can have a tensile strain of up to 5% at its ultimate load whereas ordinary concrete is a quasi-brittle material with low tensile strain capacity that can withstand up to 0.015% tensile strain on average. The large strain development coincides with fine multiple cracks, therefore the material is proposed as a promising durable cement-based composite for structural elements. This is due to the fine multiple cracks that develop under tensile loading which eliminate or decrease the rate at which chlorides, water or gaseous substances penetrate the cracks (Moriyama et al., 2009). This decrease in corrosive substances can lead to less maintenance needed for structural elements and an increase in the service life of reinforced concrete (RC) structures.

In the early stages of development of this cement-based composite the best utilisation will be in applications for structural elements where earthquake resistance is required or as a repair material for structural concrete elements. When a material is used as a repair material the durability aspect is of intrinsic value. The utilisation of SHCC as a repair material improves the service life of structures such as continuous pavements, bridge decks, wall panels and an inner layer of a water channel, since the maximum crack widths are shown to be less than 100 µm (Lepech & Li, 2005).

One of the critical properties for good durability of concrete or fine grain mortar is quantified by the width of the cracks that result under tension. Structures that consist of SHCC as a building material or as a repair material will receive less maintenance in its service life if the crack width is limited to a certain size to prevent the ingress of corrosion inducive substances. There are several different aspects that must be investigated when a new material is developed. Firstly, the cement-based material's tensile and compression behaviour must be investigated. Secondly, an in depth research study must be performed to determine what the behaviour of the material is when subjected to certain conditions coinciding with the material's application before it can be used in the industry. One of the aspects that is of importance is the time-dependant cracking behaviour of this cement-based composite under tension. These effects such as creep under a sustained load are inevitable and can be simulated under laboratory conditions to be able to quantify the time-dependant cracking behaviour of SHCC and to evaluate the quantitative results from the experimental study.

1.2 Aim and Scope

The results that are depicted in this thesis focus mainly on establishing data that can resemble the cracking behaviour of SHCC in tension in terms of crack width and to be able to use the results in future research projects. The cracking behaviour can be described in terms of the average crack width, number of cracks and other statistical properties. The definition given for the terminology of cracking behaviour will be used throughout this thesis. The tests that were conducted to quantify the cracking behaviour were quasi-static uni-axial tensile tests with varying loading rates and sustained tensile loading tests with varying loading percentages, relative to the ultimate tensile stress determined from the loading rate corresponding to a 0.001 /s strain rate. The results determined from these experiments can be incorporated in future research projects by developing a constitutive numerical model to simulate and predict the time-dependant cracking behaviour either when looking at the utilisation of this material as a structural building material or as a repair material.

1.3 Outline of Contents

Chapter 2 consists of a background study of SHCC. This chapter describes the behaviour of the composite on a micro-mechanic level of the matrix/fibre interface. A background study of research about the time-dependant effects of the cement-based material. Furthermore, research done on the cracking behaviour of Fibre Reinforced Cement-based Composites (FRCC).

Chapter 3 describes the preparation of the test specimens and the measuring instruments used to obtain the quantitative data for the cracking behaviour. Furthermore, a description of the experimental framework is given which includes the experimental research, setup and program for the individual tests performed.

Chapter 4 reports on the basic material properties found for the quasi-static uni-axial tensile tests as well as for the sustained tensile tests with their respective discussion.

Chapter 5 reports on the framework about the cracking behaviour as well as the results obtained from the two types of tests performed. This chapter also provides a discussion about the results of the cracking behaviour.

Chapter 6 is a brief summary with conclusions about the results obtained from the respective experiments performed as well as recommendations for future developments.

CHAPTER 2

BACKGROUND STUDY

In this chapter the micro-mechanical behaviour that contributes to the phenomenal strain hardening behaviour coinciding with the development of multiple fine cracks is discussed and a brief description is given about research that has been performed on the cracking behaviour of SHCC as well as the time-dependant behaviour of a typical cement-based material.

2.1 Background of SHCC

SHCC has been shown over the past few years to have crack widths, under tensile loading in the strain-hardening phase, smaller than 100 µm and with a fibre content of less than 2 % by volume (Li, 1992). SHCC is a ductile cement-based composite which exhibits strain-hardening properties. Strain-hardening is found when the tensile stress increases after the first crack with an increase in strain as shown in Figure 1.

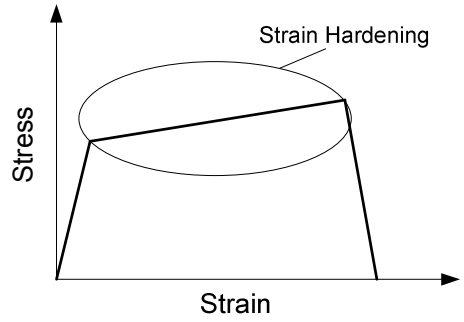

Figure 1. A stress-strain graph illustrating the strain-hardening of SHCC under tensile loading

Figure 1 clearly shows that SHCC exhibits three phases. The first phase is the linear elastic behaviour of the material representing the cement-based matrix. The second phase, strain-hardening, starts when the first crack occurs. The second phase includes the formation of fine multiple cracks. Phase Two is of importance for the investigation of the cracking behaviour of the fibre reinforced cement-based composite. The third phase, tension softening, is where the localisation of a crack or multiple cracks occur either from fibre fracture or fibre pullout or a combination of both which leads to the failure of the material. Boshoff (2007) showed that for SHCC the loading rate plays a significant role on the first cracking stress. This attribute can lead to different cracking behaviours when loaded with different loading rates or even with sustained loading. The dependency of the loading rate on the cracking behaviour for FRCC will be discussed later in this chapter.

From the research performed on SHCC there are limited publications about the tensile creep of SHCC. However, when looking at results of creep under tensile loading there are three mechanisms contributing to the time-dependant behaviour of SHCC (Boshoff, 2007). The first mechanism is matrix creep. This is well-known that an ordinary cement-based composite, like ordinary concrete, also resembles creep behaviour. The second mechanism is the time-dependant crack initiation which is the increased number of cracks developing over the highest tensile stressed area and the third is the time-dependant fibre pull-out that is directly linked to the matrix/fibre interface. These mechanisms are described in full in Boshoff (2007). Boshoff et al. (2008) showed that when SHCC is subjected to a sustained tensile load the cracking behaviour differs from that of quasi-static tensile tests. The cracks widen significantly after a certain time period under a sustained load.

2.2 SHCC Constituents and Fibre Behaviour

SHCC consists of the following constituents: water, aggregate, cement, fly ash and Polyvinyl Alcohol (PVA) fibres. A super plasticiser and a viscosity modification agent are added to ensure the correct workability. The fibre content is of utmost importance. The PVA fibres are added as a percentage of the total volume of the mix. The critical or

minimum fibre volume required to achieve strain-hardening is denoted as V_f^{crit}. Li (1993) showed for a specific mix that if the volume of fibres is above the V_f^{crit} the strain at peak resistance increases by 2 orders with a magnitude of 6% relative to specimens with the same matrix except without fibres. The PVA fibres are relatively expensive which increases the cost of this material relative to ordinary concrete. Kamal et al. (2008) showed that when the amount of polyethylene (PE) fibres, which can also lead to strain-hardening, is varied with 0.5 %, 1.0 % and 1.5 % by volume the number of cracks increases over the observed area and also the strain capacity increases. For the different fibre volume percentages the strain corresponding to the ultimate stress was measured as 0.58 %, 1.76 % and 2.8 % respectively. Thus the minimum amount of fibres must be used to ensure that the mix is optimal in terms of strain capacity to ensure that the pseudo strain-hardening properties will be maintained and guarantee cost effectiveness.

The mixture constituents that Boshoff (2007) used for the time-dependant experiments are summarised in Table 1. The type of strain-hardening response is dependant on the ratio and amount of materials used. There is a high variability in terms of the strengths, strain capacity and performance of the composite when the same mixture proportions are used in different countries. Thus the mixture proportions, especially for the admixtures, must be optimised to ensure an optimal SHCC mixture for locally available materials.

Table 1. SHCC constituents

Constituents	Ratio / Type
Water/binder ratio	0.40
Aggregate/binder ratio	0.56
Cement	Portland CEM I 42.5
Fly ash	Ratio of 1:1 by mass of cement
Sand	Fine sand with particle size of less than 600 µm as the aggregate
Fibres	PVA-RECS 15 fibres with a length of 12 mm and a 40 µm diameter added at 2 % by volume

Figure 2 indicates the important properties that characterise the fibres and the matrix and also the fibre/matrix interface. These properties are used to optimise the performance and

characterise the behaviour of SHCC. These properties will be used in this chapter to explain certain aspects of the cracking behaviour of SHCC under tensile loading.

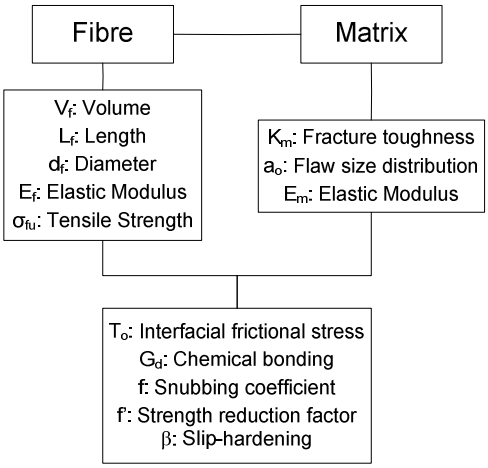

Figure 2. The fibre, matrix and interfacial properties

The multiple cracks and enhanced tensile ductility are achieved when the fibres pull out rather than rupture. The bridging properties of the fibres over a crack can be explained by the σ-δ curve (Li, 2002) shown in Figure 3.

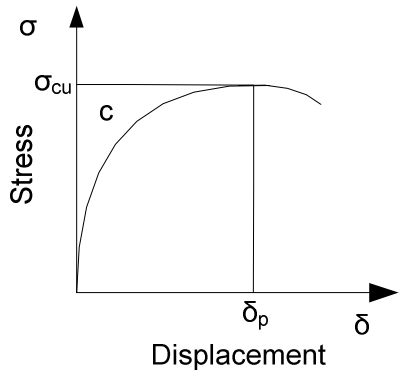

Figure 3. The σ-δ curve and the concept of complementary energy (area labelled C),

(Li, 2002)

THE TIME-DEPENDANT CRACKING BEHAVIOUR OF SHCC

The area marked with C in Figure 3 indicates the complementary energy of SHCC under tensile behaviour. This energy is related to the pseudo strain-hardening properties. A larger complementary energy will give rise to an enhanced strain-hardening phase. The complementary energy is the energy that is needed to break the bonding between the fibre and matrix interface. If the interface between the fibre and matrix is weak, then the fibres will pull out, resulting in a low strength σ_{cu}. When the fibre\matrix interface is to strong then the fibres cannot pull out resulting in the rupture of the fibres and a small value for the opening of the cracks, δ_p. A high chemical bond between the fibres and the matrix leads to a low δ_p value. In both these two cases the complementary energy will be small. Redon et al. (2001) claimed that the interfacial bond for hydrophilic fibres is around 3.8 to 5.9 MPa. These fibres also have a high chemical bond which must be broken to ensure fibre slippage (Lin et al., 1999). Higher surface coating content (between 0.8 % and 1.2 % by weight of fibres) tends to lower the interface, chemical and frictional bond properties to a level that causes the critical fibre volume fraction to drop (Li, 2002).

The crack saturation in a tensile loaded specimen can be linked to the performance requirements, namely stress performance index and the energy performance index (Li et al., 2001), which in turn can be related to the mix proportions. These two indices can be described as follows (Li et al., 2001): The first index requires that the first cracking stress must be lower than the fibre bridging stress over a cracked plane in order to ensure so-called steady state cracking. The second index requires that the energy balance must be optimal in terms of energy required and supplied during the steady state cracking. Equation 1 gives the mathematical expression for the first index and Equation 2 gives the mathematical expression for the second index.

$$\left(\sigma_{fc}\right)_i < \sigma_{peak} \qquad \text{Eq. 1}$$

$$J_{tip} < J_b^{'} \qquad \text{Eq. 2}$$

The parameter $(\sigma_{fc})_i$ refers to the first cracking stress and σ_{peak} refers to the maximum fibre bridging stress. With reference to Figure 4 these two parameters are shown as the area between the deviation from the elastic part of the curve and the turning point or peak of the curve. The area marked as C in Figure 3 is represented as the parameters J_{tip} and $J_b^{'}$ in Figure 4. The parameter J_{tip} is the energy needed from the matrix crack toughness to resist the crack propagation and the parameter $J_b^{'}$ is the net energy available for the cracks to propagate. Figure 4 is a simple illustration of the energy indices.

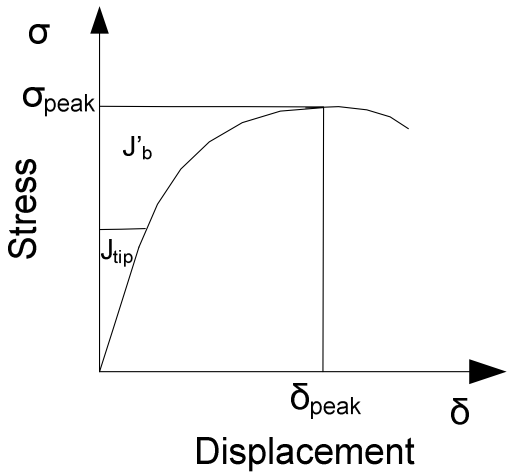

Figure 4. Energy performance indices (Li et al., 2001)

A link between the bridging stress and the opening of the crack δ can be done with a shear-lag analysis. This analysis can be studied further from the article of Krencher & Stang (1988). Li (1993) presented a function linking the stress of the bridging fibre, σ_s, and the crack opening, δ, for fibres that are aligned normal or inclined to the crack plane. Equation 3 is used to describe the micro mechanics of the fibre bridging stress relative to the opening of the cracks for fibres that are normal to the crack, whereas Equation 4 is used to describe the inclined fibres. Figure 5 a) indicates a fibre that is normal to the crack and b) shows a fibre inclined to the crack. The parameter z is the distance from the edge of the crack plane to the centroid of the fibre and Φ is the inclination angle of the fibre relative to a line

perpendicular to the edge of the surface discontinuity or crack plane. The fibre properties include the fibre elasticity modulus, tensile strength, length and diameter and the interface properties include the cohesive strength or the fracture and frictional properties.

$$\sigma_s(\delta, z) = \text{fnc}(\delta, z; \text{Fibre properties}; \text{Interface properties}) \quad \text{Eq. 3}$$

$$\sigma_s(\delta, \varphi, z) = \text{fnc}(\delta, \varphi, z; \text{Fibre properties}; \text{Local fibre/matrix interaction properties}) \quad \text{Eq. 4}$$

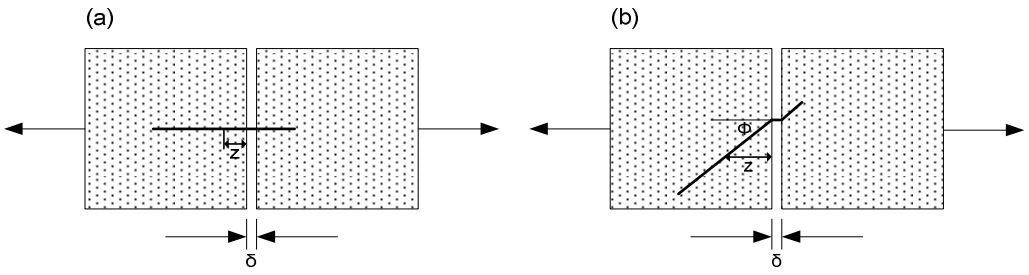

Figure 5. (a) Single fibre normal pull-out; (b) Inclined fibre pull-out (Li, 1993)

Slip-hardening is the effect of abrasive material from the fibre surface being scraped off the fibre by the surrounding matrix when the fibres are under tensile stress. This abrasive material surrounds the fibre increasing the interfacial frictional shear stress (Boshoff, 2007). Li & Chan (1993) determined that the interfacial frictional bond strength increases under load with time and is increased by the slip-hardening effect.

Fibre pull-out tests were performed by Boshoff (2007) and Redon et al. (2001). Tests from Boshoff (2007) showed that fibre rupture increases with increasing embedment length. From the tests that Boshoff (2007) performed, the embedment length limit, that will lead to fibre pull out and not fibre rupture, was defined to be approximately 1.4 mm. Rate displacement tests of 0.01 mm/min to 100 mm/min was used to perform the fibre pull-out tests. Each rate was increased with an order of ten. The tests showed that for the above specified embedment length, the increase in the displacement rate increased the occurrence

of fibre rupture. From these fibre pull-out tests Boshoff (2007) concluded that the fracture behaviour will be different with different loading rates. Results from Boshoff et al. (2008) showed that for sustained tensile loading tests and quasi-static tensile tests the crack behaviour change as a result of different stress histories. Therefore, the fibres play a significant role in the cracking behaviour when subjected to quasi-static or sustained tensile loading.

2.3 Cracking Behaviour

When SHCC is subjected to tensile loading or bending multiple cracks occur after the first crack has developed (Boshoff, 2007). These cracks lead to properties such as the ductility, toughness, fracture energy and strain-hardening (JCI-DFRCC Committee, 2003). Wu & Li (1995) indicated that the multiple crack formation is a function of the applied load. When the applied load is increased there is an increase in the number of cracks forming over the area of observation when the composite is in the strain-hardening phase. They also indicated that the first or last crack is not necessarily the localisation crack.

These multiple cracks are spaced closely and evenly. Lepech & Li (2005) showed that the crack spacing is between 2 and 5 mm at saturation with reference to their mix proportions. Boshoff (2007) showed that for five different loading rates which differ with a factor of ten, the crack spacing was 1.2 mm and 1.8 mm corresponding with the lowest rate of 0.104 mm/s and the highest rate of 10.4 mm/s respectively. The strain rate has a significant impact on the first cracking stress, strain capacity and the cracking behaviour. Thus, the effect of the strain rate on the cracking behaviour must be fully understood when the time-dependant tensile cracking behaviour is quantified.

Lepech & Li (2005) showed that for tests performed on dogbone specimens a small number of closely spaced cracks form and the width of the cracks reach a maximum of 60 µm at a strain of 0.8%, after which more closely spaced cracks form and also reach a maximum crack width of 60 µm. With this information the crack width can be quantified as a material property rather than a structural property. The material property is due to the interface

between the fibres and the matrix while in reinforced concrete the structural property is explained with the reinforcement ratio. Lepech & Li (2005) also mention that the crack width is independant of geometrical dimensions.

Under the stress-strain curve the energy absorption of the composite is given. The stress which gives rise to the first crack must be greater than the strength of the matrix, but smaller than the capacity of the bridging stress of the individual fibres. The steady state cracking is achieved if the requirements given in Section 2.2 are fulfilled. This steady state cracking results when cracks widen uniformly over a crack plane and in the case of SHCC most of the fibres remain unbroken. This crack formation is not achieved in ordinary concrete which is a quasi brittle material, where unstable Griffith cracks occur (Li, 1993). At the tip of the crack to the opening of the crack the stress which the fibres transfer to bridge the gap between the crack planes, range from zero to the maximum tensile stress that is applied (Li, 1993). The cracking is found at weak zones in the composite. The crack width can be determined with Equation 5 in terms of the fibre volume, the interfacial bond stress, stiffness of the matrix and fibre as well as the diameter and length of the fibre.

$$w_c = \frac{\tau_0 L^2}{E_f d\left(1+\frac{V_f E_f}{(1-V_f)E_m}\right)} \qquad \text{Eq. 5}$$

The model presented above can be further developed and can include other properties such as the slip-hardening coefficient β which leads to the linear behaviour of the interfacial bond stress, τ, as shown in Equation 6 which in Equation 5 is considered as a constant, τ_0. The interfacial bond stress is described by Equation 6.

$$\tau = \tau_0\left(1+\beta\frac{S}{d_f}\right) \qquad \text{Eq. 6}$$

The parameters S and β describe the relative displacement between the fibre and the matrix in a crack plane and the non-dimensional slip-hardening coefficient respectively. This linear model that was introduced by Bao and Song (1993) include the frictional slide shear stress τ_0 at the instance when S is equal to zero, meaning that there is no relative displacement between the fibre and matrix. The parameters S and β are dependant on the fibre/matrix interface and can be determined experimentally. A full description of the procedure to determine the slip-hardening and frictional shear stress coefficients can be found in Lin & Li (1997). The incorporation of the slip-hardening coefficient leads to the decrease of the critical fibre volume which in turn decreases the cost of the material. Equation 7 can be used to determine if the slip-hardening has a significant effect on the interfacial properties of the composite relative to the type of fibres used (Lin & Li, 1997). The parameters L_f and d_f describe the length and the diameter of the fibre respectively. If the following ratio is larger than 2 the influence is significant and must be taken into account.

$$\frac{\beta L_f}{2d_f} > 2 \qquad \text{Eq. 7}$$

A model that was derived by Aveston et al. (1971) includes the first crack strain. The crack width can be expressed with the aid of Equation 8. The cracks will be spaced between the parameter x' and 2x'.

$$x' = \frac{E_m d_f \varepsilon_{mu} V_m}{4\tau V_f} \qquad \text{Eq. 8}$$

The matrix and fibre are denoted with the subscripts m and f respectively. The first crack strain ε_{mu} can be expressed as shown in Equation 9.

$$\varepsilon_{mu} = \left[\frac{24 V_f^2 \tau \gamma_m E_f}{E_c E_m^2 d_f V_m} \right]^{\frac{1}{3}} \qquad \text{Eq. 9}$$

In Equation 9 the subscript c denotes the composite. Equations 8 and 9 can be used to calculate the maximum crack width w as shown in Equation 10.

$$\text{w} = \varepsilon_{mu} (1+\alpha) x' \qquad \text{Eq. 10}$$

Where $\alpha = E_m V_m \big/ E_f V_f$

The model was derived by Aveston et al. (1971) for continuous fibres and does not apply for discontinuous, short, random, three dimensional orientated fibres.

In Figure 6 the tensile response of a pseudo strain-hardening FRCC is illustrated. Li (1992) indicated that the behaviour of the FRCC has a linear elastic phase, two strain-hardening phases and then a strain softening phase. The strain hardening phase as described in Section 2.1 has in effect two separate phases. The first part marked as A describes the forming of new multiple cracks with increase in strain while the existing developed cracks reach a maximum width. The area marked with B indicates the saturation of the specimen in terms of crack. For design purpose the strain should be limited to $\varepsilon_{intermediate}$.

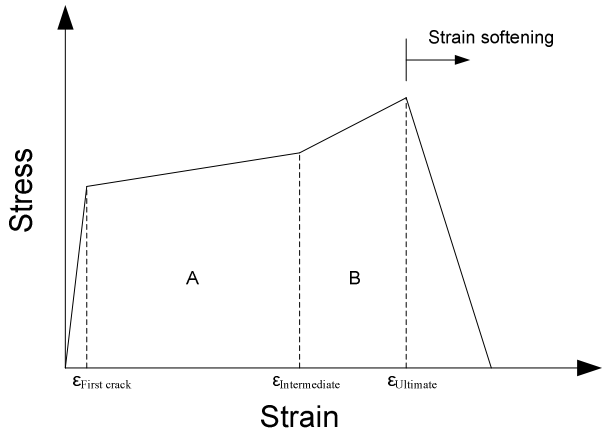

Figure 6. Tensile response of a pseudo strain-hardening FRCC (Li, 1992)

Li et al. (2001) determined crack widths experimentally with a video microscope that was magnified 50 times when the test specimens were unloaded. They found that the crack width that was measured after unloading was approximately 70% of the total opening crack width at peak load. The elastic recovery of the fibres, which bridges across the cracked plane, results in the closing of some of the cracks (Li et al., 2001). The crack width and the spacing of cracks were determined at the ultimate strain. The range of the determined ultimate strain for specimens loaded in tension was between 1.4 % and 4.6 % and with crack spacing of 11.5 mm to 1.8 mm. The average crack width was determined to be between 80 µm and 160 µm.

Jun & Mechtcherine (2008) performed tests on a single fibre as well as cyclic tests on dumbbell specimens. The study showed for the cyclic tests that the irreversible deformation was 70 % of the total deformation at a strain of 0.5 %. Jun & Mechtcherine (2008) performed creep and pull-out tests on a single fibre. The creep tests were performed at three stress levels. These three levels were 25 %, 50 % and 75 % of the ultimate tensile strength of the fibre. The creep results showed that the initial creep strain after loading is significantly high. Thereafter, the increase in strain after several hours is significantly lower.

Cracking in concrete is inevitable when subjected to tensile or flexural loads. However, the cracking can be controlled with reinforcement. Maalej & Li (1996) used a layer of SHCC in the tension zone of a RC beam and normal concrete in the compression zone. This hybrid RC beam limited the crack width, under service loads, to 51 µm and with the member being overloaded the crack width at the ultimate load could be limited to 193 µm. The crack width was controlled by the SHCC layer.

Weimann and Li (2003) have shown that under large strains the crack width remains 60 µm for a particular mix composition. Boshoff et al. (2008) showed that under sustained loading of 60 % of the ultimate resistance stress for a specific mix, the width of the cracks reached 300 µm in only 3 weeks and the creep tests gave rise to fewer but wider cracks. The conclusion was made that the crack width is dependant on the loading history. However, the test specimens were notched and the crack widening isolated as the dominant time-dependant deformation.

2.4 Time-Dependant Effects: Creep and Shrinkage

Creep of ordinary concrete has three phases. Figure 7 shows the three phases on a strain versus time graph. The secondary creep is referred to as steady state creep. The terminology refers to the creep rate which is constant. Creep fracture occurs when the concrete cannot withstand the applied stress and the specimens fail in the tertiary creep phase (Rüsch, 1960).

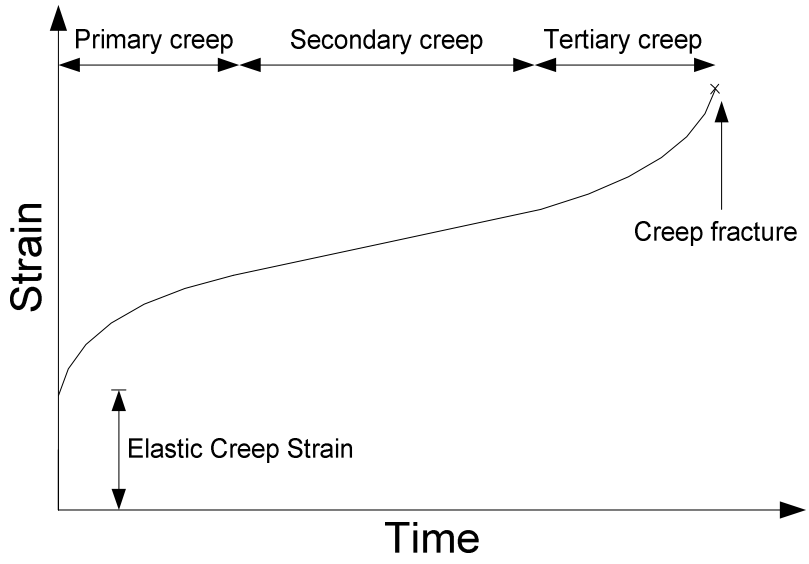

Figure 7. Phase representation of creep over time for ordinary concrete

Creep fracture occurs when a sustained load which is applied to ordinary concrete is above the creep fracture limit. A creep fracture limit was proposed by Zhou (1992) for notched beams of ordinary concrete in flexure. These flexural tests were performed with force control and displacement control. The first step was to find the normal or reference load-deflection response for the flexural members under displacement control. The force control was initiated on flexural members to keep the load at a sustained level. Sustained loads at 92%, 85%, 80%, and 76% of the ultimate resistance load, from the reference load-deflection response curve, were used. Failure for all four sustained loads occurred and is indicated with an x in Figure 8. Further tests established that the creep fracture limit is at 60% of the ultimate resistance load for ordinary concrete. The creep fracture for SHCC is still undefined.

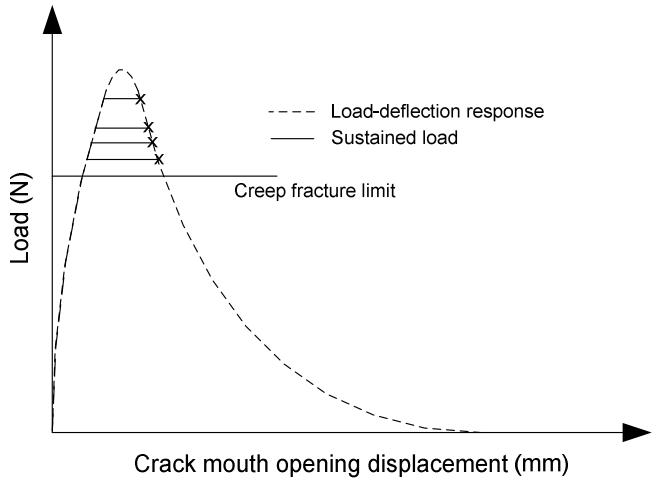

Figure 8. Load-deflection response showing the failure of four sustained loads at 92%, 85%, 80%, and 76% of the ultimate resistance load (Zhou, 1992)

Figure 9 indicates that for a certain sustained load applied relative to the ultimate resistance load the creep strain is constant until a certain load ratio, where after the response deviates and shows non-linear behaviour. This deviation point is known as the non-linear creep load ratio, λ.

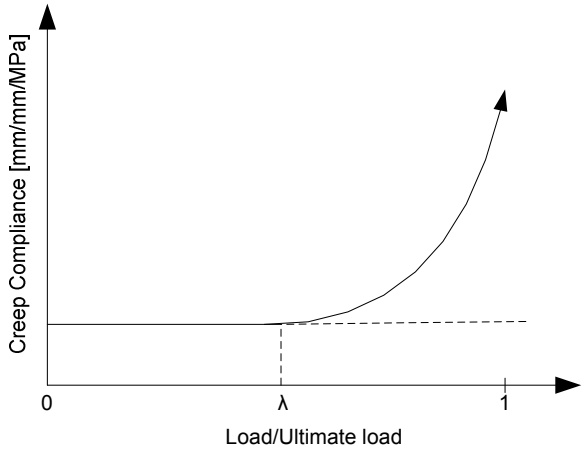

Figure 9. The non-linear behaviour of creep relative to the applied load ratio

(Boshoff, 2007)

Rouse & Billington (2007) determined total creep and basic creep of SHCC undergoing a compression load. Basic creep is when the drying creep is subtracted from the total creep and was determined with specimens that were sealed. The total creep was measured on unsealed specimens with similar geometry. The drying creep was determined with the basic creep subtracted from the total creep. Experiments were performed on two different SHCC mixtures. The first mixture of SHCC consisted of an ordinary paste of cement and silica fume and the second mixture had fine sand as aggregate which is referred to as the mortar mix. Both mixtures had the same fibre content. The results indicated that the basic creep was much higher for the ordinary paste mixture than for the mortar mixture.

2.5 Summary

The development of a numerical model in a future research project that can predict the cracking behaviour of SHCC is of importance to be able to use the material effectively. However, meaningful data must be gathered to construct such a model. It has been reported that the multiple crack formation provides numerous cracks with widths normally smaller than 100 µm thus the material can be used for a number of purposes (Li, 2001).

There are numerous works published, (Wu & Li, 1995), (Li, 1992), (Boshoff et al., 2008), (Weimann and Li, 2003) about the crack width and spacing of cracks that develop under quasi-static uni-axial tensile tests. However, there is no concrete evaluation of the cracking behaviour of SHCC with respect to different quasi-static rate tests. Although only a few research reports about the time-dependant behaviour of SHCC have been published, for example Rouse & Billington (2007), Jun & Mechtcherine (2008) and Boshoff (2007), the literature provided insight into the understanding of the rate effect on the material properties and the fibre behaviour as well as the effect of different sustained loads on the time-dependant behaviour and mechanisms contributing towards the strain-hardening phenomena.

The literature gave rise to the need to investigate the rate effect as well as sustained tensile tests to address the time-dependant cracking behaviour of this material. Therefore, in this

thesis loading in the linear and non-linear creep regions is performed to determine the behaviour of the material under different loading regimes.

CHAPTER 3

EXPERIMENTAL FRAMEWORK

3.1 Introduction

The ductile behaviour of SHCC is determined by the fibres and the fibre/matrix interface. The constituents and their proportions contribute to the strength and ductility of the composite. Therefore, in this chapter, an explanation is provided for the proportions used for the SHCC mix and an optimal quantity of admixture was determined to obtain maximal strength and ductility performance for this HPFRCC.

In Chapter 2 the cracking behaviour, specifically the crack widths, was discussed for SHCC. It is well known that the widths of the cracks that develop under a tensile load for this FRCC are smaller than 100 µm (Li, 2001). Hence, an objective and accurate measurement device is needed to analyse this relative fine cracking behaviour of this composite. The measurement device used to determine the crack widths for the uni-axial and sustained tensile tests is described in this chapter.

The chapter ends with the discussion of the experimental procedure and program for the quasi-static and sustained tensile tests.

3.2 Specimen Preparation

The SHCC mix used by Boshoff (2007) was modified in terms of the proportions of the constituents. The combination of the constituents that was used induced a strain capacity of more than 4 % and an average ultimate stress of more than 4 MPa when loaded with a strain rate of 0.001 /s. This is considered as a “normal” loading rate, which causes failure of

test specimens after 2 to 5 minutes. The modification of the constituent proportions was introduced by the RILEM Technical Committee 208 Sub-committee 2: High Performance Fibre Reinforced Concrete. This modification ensured that research done on SHCC with regard to the cracking will be comparable to other research work. The problem arose that each admixture, namely the super plasticiser and viscous modification agent which are used from local suppliers, differ for each country. Therefore a test series was performed to determine what the optimal amount of each admixture must be to induce a strain capacity of more than 4 % and with a reasonable good repetition of stress strain response results. From this test series it could be established that the optimal amount in terms of percentages for the viscous modification agent and super plasticiser were 0.075% and 0.4% of the cement weight respectively for the local admixtures. The cement was supplied by PPC South Africa. The fly ash is marketed as Dura Pozz by Ash Resources. The aggregate that was used is fine sand which has particle size smaller than 600 µm. In Figure 10 the grading of the aggregate is shown. The fibres were supplied by Kuraray, Japan. The SHCC mix constituents, ratios and proportions that were used for the quasi-static tensile tests and sustained tensile loading tests are given in Table 2. The cement and fly ash are referred to as the binder.

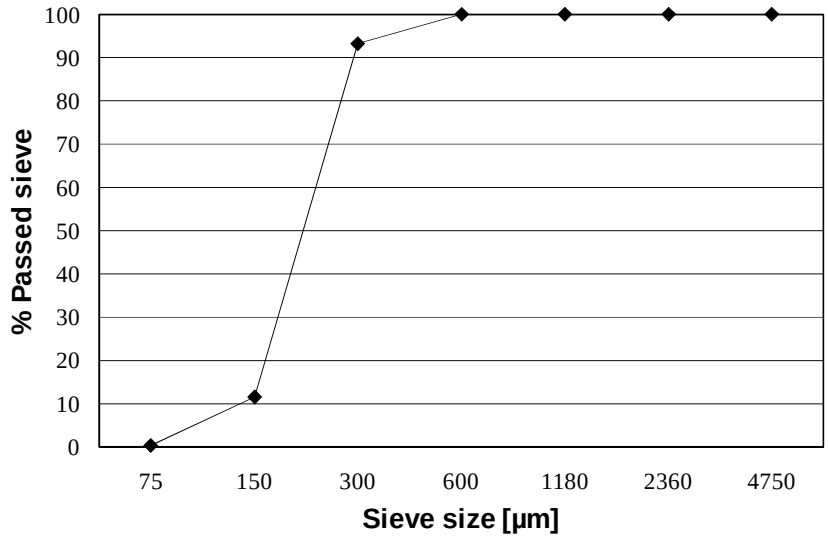

Figure 10. Aggregate grading: Local silica sand type Console number 2

Table 2. SHCC constituents, ratio's and mix proportions

Constituents	Ratio / Type	Mix proportion (kg/m3)
Water/binder ratio	0.33	-
Aggregate/binder ratio	0.46	-
Water	-	395
Cement	Portland CEM I 42.5	550
Fly ash	Ratio of 1:0.85 by mass of cement	650
Sand	Particle size < 600 µm	550
Fibres	PVA-RECS 15 fibres: Length:12 mm Diameter: 40 µm 2 % by volume	26
Viscous modification agent	Aqua Beton 0.075% of cement	0.413
Super plasticiser	Premia 100 0.4% of cement	2.2

The proportions given in Table 2 were decreased proportionally to a 5 litre mix. The mix was used for twelve dogbones, one cube and a flow table test. The mix constituent weight was measured to the nearest gram. A Hobart type mixer was used for the mixing. Before the mixing process started the mixing drum was cleaned with a wet cloth to ensure that the drum was saturated with moisture to decrease the loss of water from the mix into the mixing drum, however still dry enough not to alter the mix ratio. The mixing process was as follows: First half of the quantity of sand was poured into the mixing drum. Thereafter the cement, fly ash and viscous modification agent was poured on top of the sand. Thereafter the remainder of sand was poured over the other dry constituents. This process was carried out to ensure that the smaller particles from the cement and fly ash were not lost during the mixing of the dry contents. The dry constituents namely, the cement, sand, fly ash and viscous modification agent were mixed together for 1 minute. After the 1 minute the water was slowly added and mixed for another minute. Thereafter the super plasticiser was added and mixed again for 1 minute. The mix was stopped and an inspection of the mix was performed to ensure that all the constituents were mixed together thoroughly. The mix was then continued and the fibres were added to the mix. The fibres

were added over a period of 1 minute to ensure that the dispersion of fibres was correct, since the fibres tend to clump when added at once. The mixing was then continued for approximately 5 minutes while the moulds where prepared for casting.

The mix was firstly tested with a flow table to test whether the rheology was correct. The test involved the procedure given in the British Standards EN 1015-3:1999 code. Part of the apparatus is a circular steel cone with top and bottom external diameters of 70 mm and 100 mm respectively and a thickness of 5 mm. The cone is placed on a table with diameter 500 mm which is connected to a turning shaft. The handle can be turned in a circular motion, whereby the table is lifted to a certain height and then dropped with a sudden motion. This enables the cement-based composite to spread over the table after the circular cone has been removed. A picture is shown in Figure 11 of the flow table used for the testing of the rheology.

Figure 11. The flow table used for the testing of the rheology

Firstly, a third of the cone is filled with the mix and then tamped ten times with a tamper in a circular motion. The tamper consists of a rigid, non-absorptive rod of circular cross-section and at the tamping face of 40 mm in diameter. The mass of the tamper is 0.250 kg ± 0.015 kg. Thereafter the cone is filled to the top and tamped in a circular motion for ten

times. The cone is removed and the table is lifted and dropped for fifteen cycles with a speed of one cycle per second. After the fifteen cycles the diameter of the flowed mix is measured at right angles of each other and the average of the two measurements calculated. Previous tests performed in the laboratory showed that the average diameter of the mix should be between 150 mm and 160 mm. This test was used as a guideline to ensure that every mix would be similar regarding the rheology which in turn would have an effect on the results obtained from the tests. After the flow test the mix was either approved or discarded.

Secondly, the mix was transferred into dogbone shaped moulds. The moulds were lined with an oil based liquid which assisted with the removal of the specimens. In Figure 12 a mould that was used for the test specimens is shown. These moulds are made of steel and have removable lids with two holes of 16 mm diameter near the ends of the lid. These holes are there to be able to let two pins pass through the specimens to ensure that there is a 16 mm diameter hole near each end of each specimen to assist with the testing procedure. The dimensions of a specimen are given in Figure 13.

Figure 12. A steel mould and lid for the test specimens with the two removable studs

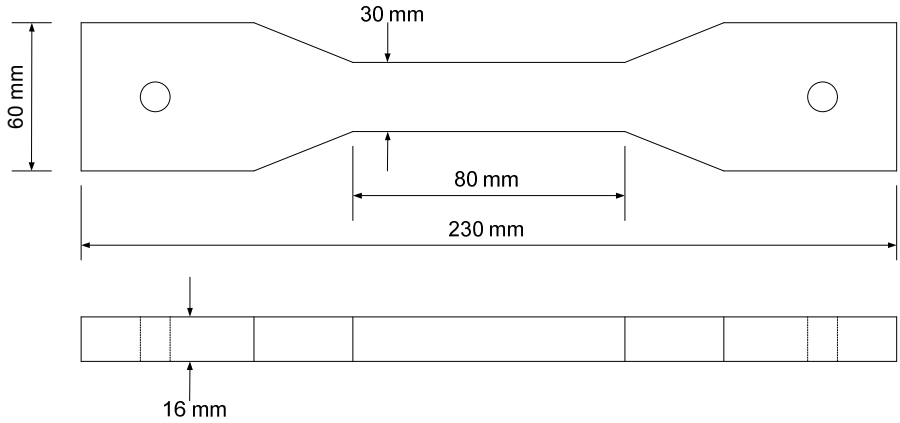

Figure 13. Dimensions of the test specimens

After the mix was cast into the dogbone shaped moulds the moulds were vibrated without the lids for at least 20 seconds. The moulds without the lids were moved to a climate room where they were left to ensure that most of the still entrapped air content would dissipate from the mixture. The sustained tensile tests were performed in the same climate room. After an hour and a half the specimens were levelled with a trowel. In this process the air bubbles that were trapped underneath the top layer of the specimens were also removed insuring a good surface finish. Thereafter the lid was put on each mould. The climate room temperature was kept at 24 ºC ± 2 ºC and a relative humidity of 65 % ± 10 %. The standard test requirement for relative humidity control is usually ± 5 %. In this case the control of the relative humidity is double that of the standard requirement. A reason for this is that the climate was not controlled properly. However, this will have a negligible effect on the results of the creep test, since the matrix creep, which is a function of the humidity, is significantly lower than the deformation resulting from the crack width and number of cracks. Figure 14 a) and b) are graphical representations of the temperature and relative humidity in the climate room from 1 day prior to the first moulds were put in the climate room until the termination of the sustained tensile tests. After 24 hours in the climate room the specimens were de-moulded and water cured at 23 ºC for a further 13 days.

Prior to testing, the specimens were removed from the water curing bath and all external water was removed using compressed air. A thin layer of ground limestone mixed with

water was painted over the observed gauge length area as shown in Figure 15. Compressed air was used to quicken the drying of the thin layer of limestone which reduced the time the specimens were exposed to the environment. Black aerosol paint was used to spray fine, black spots onto the white limestone layer. Figure 16 shows an enlarged view of the pattern on the specimen. This procedure is required by the non-contact optical 3D digital deformation measuring system, ARAMIS, which was used to determine the crack widths, and will be explained in more detail in Section 3.3.

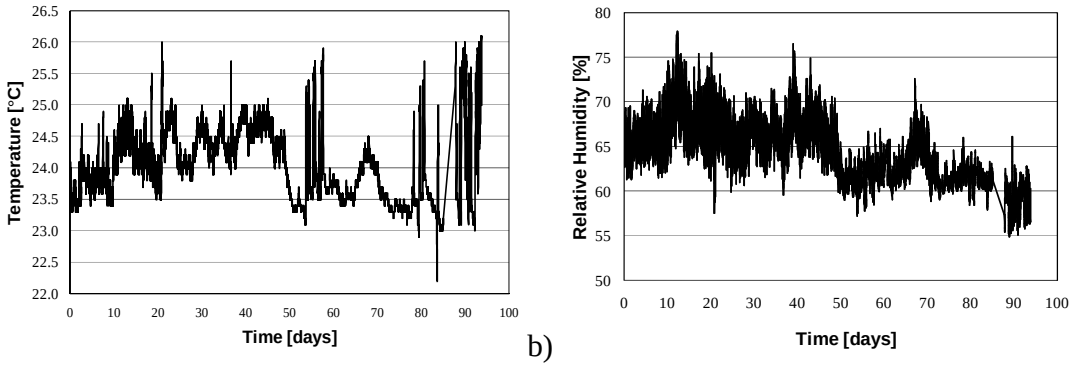

a) b)

Figure 14. a) The temperature in the climate room and b) The relative humidity of the climate room

Figure 15. Specimen with painted layer of limestone

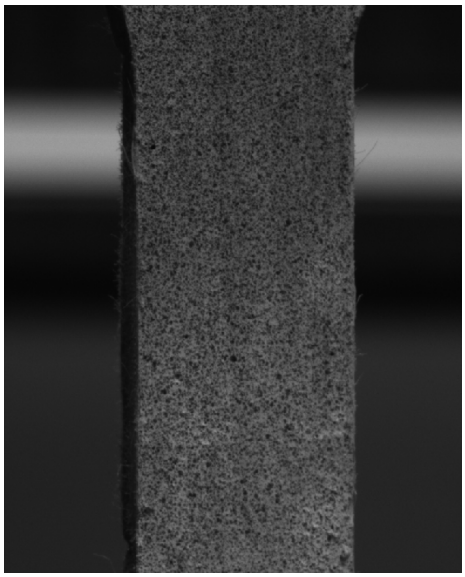

Figure 16. Enlarged view of the stochastic pattern on the specimen

3.3 Digital Deformation Measurement System

The system that was used for the crack width measurement is called ARAMIS. The system was developed by GOM Optical Measuring Technics and the company is based in Germany. The system is used as a non-contact optical 3D digital deformation measuring device. The system comprises of a high-performance PC system with the ARAMIS version 6.1 software as well as a sensor with two cameras and a tripod for secure and steady holding of the sensor. During the test the sensor takes digital photo's and stores each image as a stage in a project. The time frame of the images can be varied between 10 images per second to 1 image per hour depending on what data are needed from the test. The sensor must be a specified distance away from the test object which is determined by the sensor type and the measuring area under consideration.

The ARAMIS software analyses each stage for each test that undergoes a certain deformation. The deformation can only be calculated with a reference stage. The reference stage is an image that was taken before the commencement of the test in the undeformed state. The deformation is determined relative to this stage. Before the analysis is performed

an area is masked that will be analysed. In Figure 17 the green area indicates the area that was masked for a certain stage.

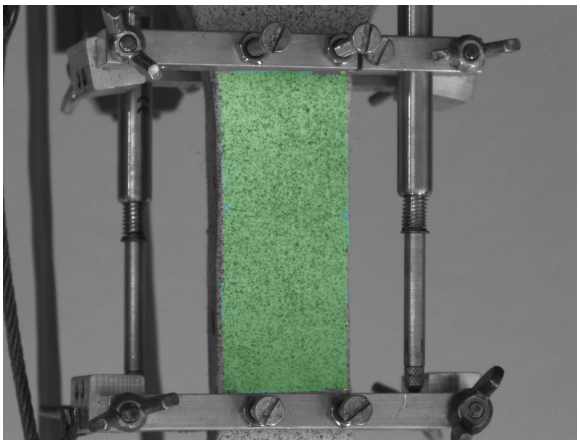

Figure 17. A masked area on a stage that was analysed

The analysed area is divided into a certain amount of pixels. The pixels are used to create grids of a certain size. These grids are called facets. The facet size is defined before the stages are analysed. The facet size for the uni-axial and sustained tensile tests was of a 15 x 15 pixels with a 2 pixel overlap and is shown in Figure 18.

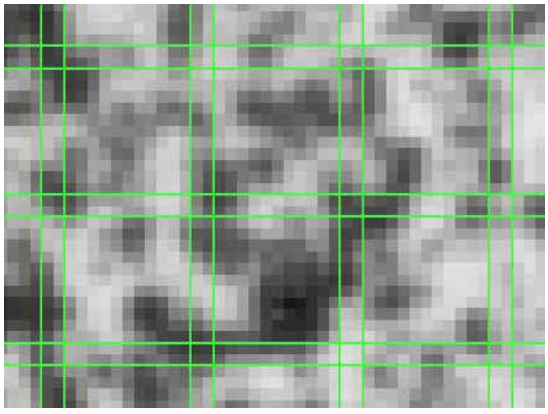

Figure 18. Facet sizes of 15 x 15 with a 2 pixel overlap (ARAMIS help file)

After the analysis of the stages the masked or analysed area is divided into a defined coordinate system. The corner and centre of each facet are then allocated with the coordinates. The stochastic pattern, described in Section 3.2, provides identifiable object characteristics. These object characteristics are observed in every facet and used to determine the deformation of the facets for each stage relative to the reference stage. With the deformation of these facets the coordinates of the grid points in the deformed state for the facets are recorded. The coordinates of the grid points in the deformed state are then exported for each stage to determine the crack width.

Different analysis tools can be used to obtain different data. The element tool called Section Line was used to obtain the coordinates of the grid points in the deformed state over the length of the analysed area in the middle of the specimen. The analysed area was 70 mm x 30 mm. The line is divided into points. These points are situated on the corners of the facets which contain the coordinates of the grid points in the deformed state. One section line was used in the middle of the specimen as shown in Figure 19 for the analysis of both the quasi-static tensile tests and the sustained tensile tests.

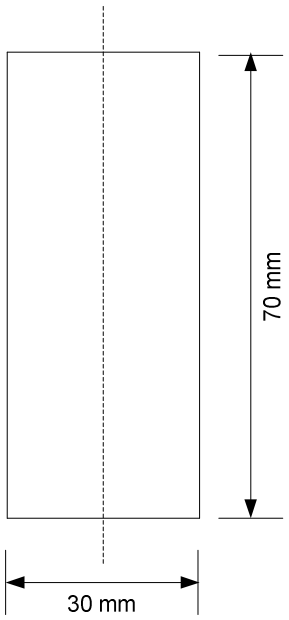

Figure 19. Position of section line on the analysed area

The one line in the middle of the analysed area represents the true tensile cracking behaviour for the tests. If one considers the steady state growth of a crack as explained in Chapter 2, the true cracking behaviour can only be considered if one line is used in the middle of the specimen and is explained as follows: The crack initiates at the edge of the specimen as shown in Figure 20. When a line in the middle of the analysed area and a line 5 mm from the two edges are considered and the average of the results of these three lines are used then this will result in incorrect results. The explanation for this is that the middle line will indicate zero crack development and the two lines close to the edge will each indicate a single crack development, at a certain strain stage. Therefore the definition of a crack in this thesis is when a crack has passed the centre of the specimen.

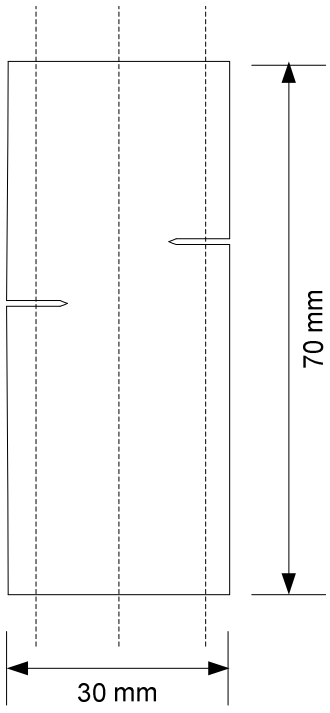

Figure 20. Idealisation of a crack growth for a specimen undergoing a uni-axial tensile load

After the analysis is performed with the aid of the ARAMIS software the cracks are shown visually with the aid of contour lines. In Figure 21 a) a specimen is shown at a certain strain

stage showing the physical cracks. In Figure 21 b) the analysed area is shown with the developed cracks in different contour colours.

a)

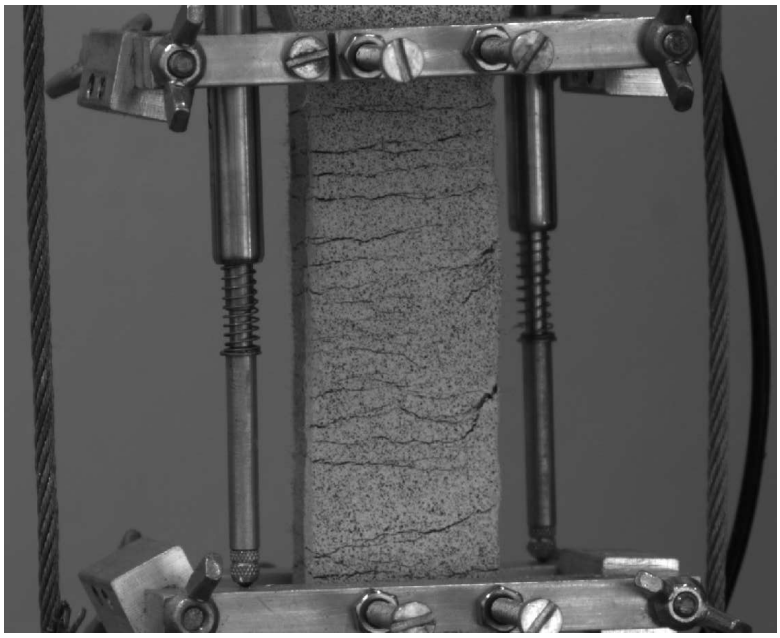

b)

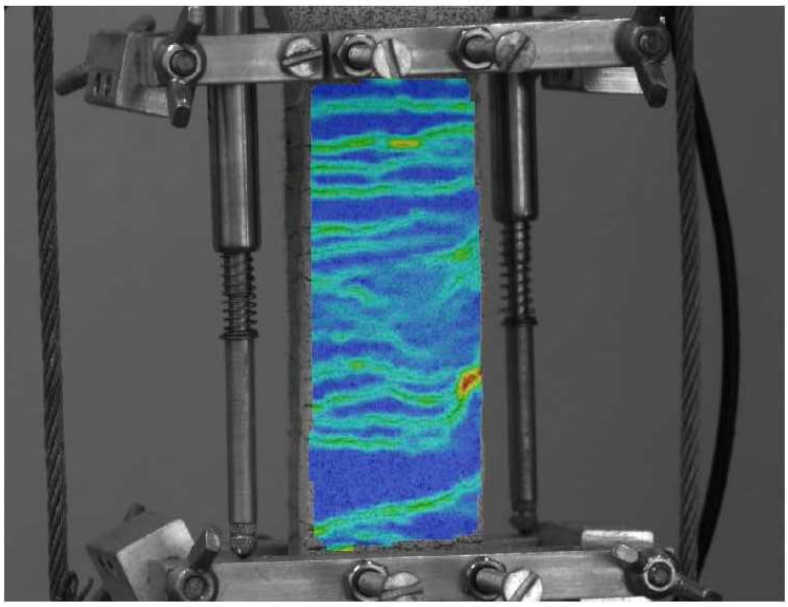

Figure 21. a) The developed cracks for a specimen at a specific strain b) The analysed area showing the physical cracks with contours with the aid of the ARAMIS software

3.4 Uni-axial Quasi-static Tensile Tests

3.4.1 Research program

The scope of this research program included rate-dependant tensile tests of uni-axial tensile specimens. These tests were performed to understand the cracking behaviour and included five different loading rates to determine what the rate effect is of SHCC in tension. The chosen loading rates were 0.0008, 0.008, 0.08, 0.8 and 8 mm/s. The lowest loading rate of 0.0008 mm/s corresponds with a strain rate of 0.00001 /s for a gauge length of 80 mm. This loading rate is normally referred to as a pseudo-static loading rate, however the highest loading rate of 8 mm/s corresponds to a strain rate of 0.1 /s for a gauge length of 80 mm and is normally referred to as a dynamic loading rate (Boshoff, 2007 and Kim et. al., 2008). The loading rate of 0.08 mm/s corresponds to a “normal” loading rate which causes an average strain rate of 0.001 /s. The stress and strain results determined from the 0.08 mm/s loading rate were used to determine the average ultimate resistance stress that was used as reference for the sustained tensile tests and will be explained in more detail in Section 3.5.

The basic material parameters were determined from these tests. For each loading rate the ultimate stress and ultimate strain were determined. The average Young’s modulus was determined for the 0.001 /s strain rate. Descriptive statistical characteristics were used to describe the crack width distributions. These statistical characteristics are essential for a model to describe the distribution of the crack widths at a certain strain percentage. The cracking behaviour characteristics will be discussed in more detail in Chapter 5.

3.4.2 Experimental methodology and setup

Tests were performed to determine what the stress strain responses for the specific SHCC mix are at different loading rates and to determine the corresponding cracking behaviour at certain strains. The data obtained to calculate the stresses and strains and the data obtained with the ARAMIS software for the cracking behaviour were logged on two different

computers. Therefore, the only way to link the stress and strain results with the cracking behaviour results was with synchronised times for the two computers.

The uni-axial quasi-static tensile tests were performed in a Zwick Z250 Universal Materials Testing Machine. It was possible to perform all the loading rates with this testing machine. The Universal Materials Testing Machine is equipped with a load cell, but a separate load cell was connected to ensure more accurate load values. The load was measured using a 500 kg HBM load cell and the loading rate was applied between the crossheads of the machine. The linear displacement over the 80 mm gauge length was measured with two 10 mm HBM linear variable differential transformers (LVDT). These two LVDTs were fixed to an aluminium frame which in turn was fixed to the specimen with small screws, as shown in Figure 22. One LVDT is in the front left of the specimen and the other at the back right of the specimen in order to calculate an averaged displacement over the gauge length. The LVDTs and the load cell were connected to a Spider8 high frequency multi-channel electronic PC measurement unit.

Figure 22. The two LVDTs connected to a frame and connected to the specimen

The two support conditions for testing the specimens were hinged and fixed. The clamps were designed for these two support conditions to ensure a rotational degree of freedom in two directions at the top, which is the stationary support, and a fixed degree of freedom at the bottom which is also the displacing support. The support conditions were chosen in this manner to ensure that over the gauge length only a tension force would be induced and no additional moments. The clamps that were used are shown in Figure 23.

Figure 23. The clamps used for the uni-axial tensile tests in the Zwick

3.4.3 Experimental program

Five different loading rates were tested and for each loading rate at least four specimens were tested. The test specimens were prepared from five separate mixing batches. The total number of specimens for each loading rate is given in Table 3.

Table 3. The number of specimens used for each loading rate test

Tensile loading rate tests						
Loading rate	[mm/s]	0.0008	0.008	0.08	0.8	8
Number of specimens	-	4	4	6	4	4

3.5 Sustained Tensile Loading and Shrinkage Tests

3.5.1 Research program

The primary objective for the sustained tensile loading tests was to determine the time-dependant cracking behaviour of SHCC. The experimental setup restricted the amount of specimens that could be tested at once and therefore the program was narrowed to determine only the cracking behaviour on specimens that were not pre-cracked. The same methodology was used as described for the quasi-static tensile tests to link the data acquired from the ARAMIS software to the corresponding strains measured over a gauge length of 80 mm for each specimen.

Three load levels were chosen for the creep tests, namely one in the elastic region and two in the strain hardening phase. The ultimate stress was determined from tensile tests at a 0.001 /s strain rate. The loading percentages chosen were 50 %, 65 % and 80 % of the ultimate resistance corresponding to the above mentioned regions. Due to the variability of the cross section the loading percentages ranged from 40 % to 80 %. Four shrinkage specimens were also tested to determine the shrinkage behaviour of the specific SHCC mix.

3.5.2 Experimental methodology and setup

For the creep tests a lever arm method was used to apply the load. The setup consists of six loading lanes. A lane can be described as two specimens in series connected to a lever arm as shown in Figure 24. This setup was designed by Boshoff (2007). The load was applied by hanging weights at the cantilevered end. The lever arm exerts a reaction force on the

specimens that coincides with a factor of roughly 4 times the applied force at the cantilevered end and can be calculated with the diagram shown in Figure 25. The exact factor for each lane was however measured by placing a load cell in the specimen position.

Figure 24. Sustained tensile loading setup

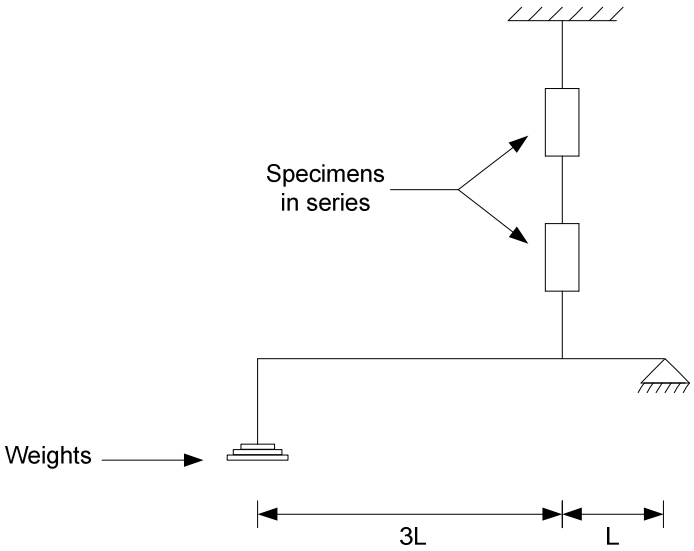

Figure 25. Schematic representation of the sustained tensile loading setup

The top and bottom specimens do however have slightly different applied loads due to self weight of the specimens and the clamps. This difference was however incorporated in the calculation of the total loading percentage for each test. With the average ultimate stress determined as 4.26 MPa a calculation was performed in order to determine what the applied weight was for each loading lane. Two loading lanes were allocated for each chosen loading percentage. Due to the variability of the cross section a nominal uniform cross section was considered of 15 mm by 30 mm to convert the stress to a load in order to calculate an estimated value for the applied mass. The true loading percentage was determined after the cross-section of each test specimen was measured.

The lever arm with the free hanging weights was lowered gradually using a hydraulic jack. Each specimen's linear displacement was measured with two 10 mm HBM LVDTs with a similar setup as described in Section 3.4.2. The clamps used for the sustained tensile loading tests were designed to simulate similar support conditions that are represented by the quasi-static tensile tests. Two of the support conditions were hinged and one support condition represented a fixed support. The top specimen was connected with a hinge support to a fixed frame which was fixed to the surrounding wall structure. The hinge support provided two rotational degrees of freedom. The bottom specimen was connected to the lever arm and had the same two rotational degrees of freedom as for the top hinge. The bottom part of the top specimen and the top part of the bottom specimen was connected with a clamp that could not rotate and resembled the bottom fixed support condition of the uni-axial tensile test. The clamps refer to two steel plates that are corrugated on the one side to better grip the specimen. The specimens were fixed to the plates using bolts. The clamp mechanism for the sustained tensile tests is shown in Figure 26. The side view of a bottom specimen is shown in Figure 26 b).

The preparation of the shrinkage specimens was performed in the same manner as described in Section 3.2 to ensure that they are exposed to the same drying conditions even though they will not be analysed using the ARAMIS system. The linear displacement was measured for each shrinkage specimen with two 5 mm HBM LVDTs fixed to the specimen as described in Section 3.4.2 and is shown in Figure 27.

a) 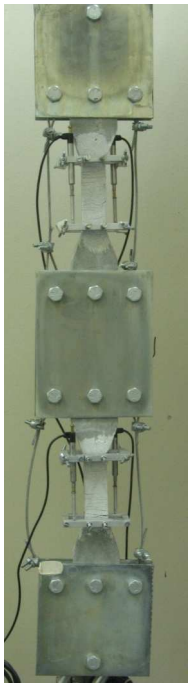 b) 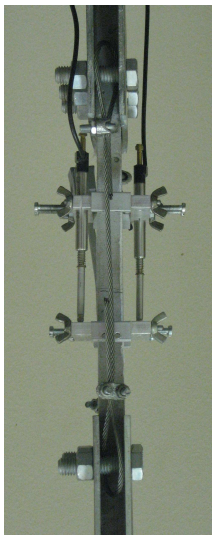

Figure 26. The clamps used for the sustained tensile tests a) front view and b) side view

Figure 27. Setup of the shrinkage specimens

3.5.3 Experimental program

A total of 30 specimens were tested for the sustained tensile tests. From the 30 specimens twelve were used to determine the cracking behaviour. Two of the thirty specimens did not crack in the observed area but cracked where the LVDT frames were connected to the specimen and therefore the cracking behaviour could not be determined. Five specimens failed before 30 seconds from the start of the test, which led to ten specimens being discarded seeing that they were connected in series. Three specimens failed between 1 and 10 minutes after the commencing of the test and therefore another six specimens were discarded. During the first 3 minutes only one specimen was recorded with the ARAMIS system. After 3 minutes the measurement device was adjusted to record the specimen that was in series with the previously recorded specimen. The adjustment took roughly 4 to 5 minutes. Therefore, the cracking behaviour could not be determined for the three specimens that fractured between 1 and 10 minutes.

The loading lanes were numbered alphabetically from A to F and the tests were numbered in chronological order. After a specimen fractured the two specimens were removed and two new specimens were loaded in the specific lane. The loading percentage and duration for each test are given in Table 4. The highlighted lines are the twelve specimens that were used to determine the cracking behaviour. After the four initial tests for loading lane F the loading percentage was slightly reduced to prevent the sudden failure found. The two specimens that cracked outside of the observed area are A1 top and A1 bottom. These two are the only specimens that reached 64 days and after this time the recording of data were stopped.

Table 4. The loading percentage and duration for each sustained tensile test

Loading Lane	Loading percentage of the ultimate stress	Total test time [min]
A1 Top	46.7 %	92650
A1 Bottom	45.7 %	
B1 Top	49.3 %	73330
B1 Bottom	40.0 %	
C1 Top	60.1 %	21920
C1 Bottom	60.5 %	
D1 Top	61.9 %	3.679
D1 Bottom	60.7 %	
D2 Top	58.6 %	24740
D2 Bottom	60.0 %	
E1 Top	78.7 %	4979
E1 Bottom	74.5 %	
F1 Top	72.7 %	0.489
F1 Bottom	75.2 %	
F2 Top	77.7 %	6.479
F2 Bottom	77.1 %	
D3 Top	61.1 %	0.239
D3 Bottom	58.8 %	
D4 Top	63.3 %	0.479
D4 Bottom	60.8 %	
D5 Top	58.6 %	0.209
D5 Bottom	58.6 %	
D6 Top	61.1 %	17460
D6 Bottom	59.8 %	
F3 Top	72.0 %	1.279
F3 Bottom	67.2 %	
F4 Top	69.1 %	0.449
F4 Bottom	68.2 %	
F5 Top	65.1 %	11840
F5 Bottom	64.3 %	

3.6 Summary

In this chapter the experimental setup, methodology and program were discussed for the uni-axial tensile tests as well as for the sustained tensile tests. A test series of uni-axial tensile tests was performed to determine the specification of an optimal mix for SHCC. The optimal mix for SHCC in terms of the proportions and ratios was determined and used for two types of tensile tests. The rate-dependant tensile tests were performed with uni-axial tensile specimens. The effect of the loading rate on the cracking behaviour was investigated

for SHCC. Different loading percentages of the ultimate tensile resistance stress, which was determined from the 0.001 /s strain rate tests, were performed to investigate the cracking behaviour under different loading regimes. The objective of the tests was to determine the cracking behaviour for both the uni-axial as well as the sustained tensile tests.

The cracking behaviour for both the rate-dependant and sustained tensile tests was determined using a non-contact optical 3D digital deformation measuring device called ARAMIS. The device consists of two cameras that took digital images of an observed area during the test. This device was used to determine the width of the developed cracks over time. In order to determine the crack width a definition for a fully developed crack was formulated that was used throughout this thesis to determine the cracking behaviour characteristics for the different tests, namely a crack that passes through the specimen centre along the loading-axis.

CHAPTER 4

TESTS RESULTS

4.1 Introduction

The main objective for the uni-axial quasi-static tensile tests was to determine the cracking behaviour for different loading rates. Boshoff (2007) showed that the different loading rates have an influence on the ultimate tensile strain and ultimate tensile stress of SHCC. The loading rate also has a significant effect on the fibre behaviour.

In this chapter the test results for the quasi-static and sustained tensile tests as well as shrinkage tests are discussed. This chapter also includes some of the basic material properties under different loading rates.

4.2 Uni-axial Quasi-static Tensile Tests

4.2.1 Basic material properties

The stress-strain response for each test coinciding with the respective loading rate is shown in Figure 28. The stress was calculated for each test specimen by dividing the recorded load by the cross sectional area in the gauge area. The strains were determined with the recorded LVDT displacement values over the gauge length of 80 mm. The strains are given as a percentage.

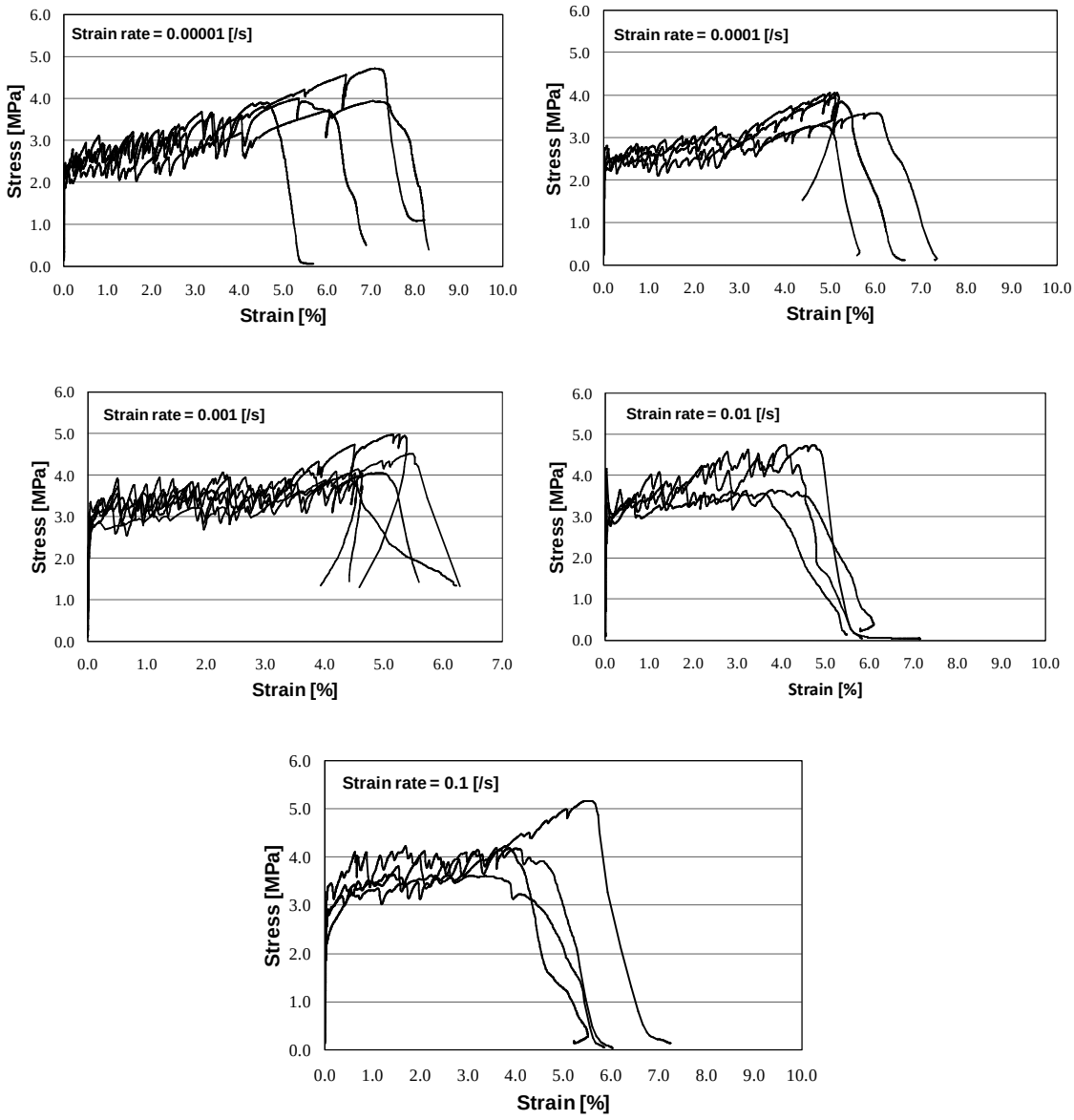

Figure 28. Stress-strain responses for each loading rate from the lowest to the highest strain rate

The highest stress that was recorded after the first cracking point of each response was used as the ultimate resistance stress. The coinciding strain for the ultimate resistance stress was considered as the ultimate strain capacity before strain softening occurred with the exception of one specimen from the 0.001 /s strain rate tests. This one test specimen

reached a maximum or ultimate stress, where after the load decreased suddenly. Thereafter, the specimen continued with increased strain and increased stress, although recording lower stress values than the maximum or ultimate resistance stress. In Figure 29 the graphs indicate the average ultimate stress and average ultimate strain for the five strain rates with the corresponding minimum and maximum values respectively.

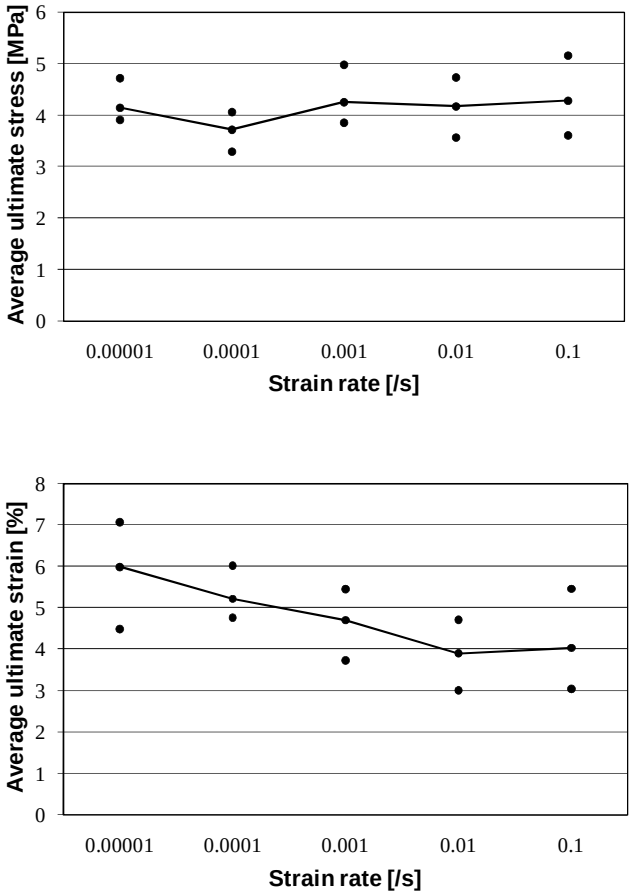

Figure 29. Average ultimate tensile stress and average ultimate tensile strain with the minimum and maximum values indicated for each strain rate

The Young's modulus (E-modulus) was determined for the 0.001 /s strain rate and the average E-modulus with the corresponding minimum and maximum values is shown in

Table 5. The average E-modulus is 12.7 GPa and was determined for five specimens and not for the six test specimens. The reason for discarding the one specimen will be made clear in Chapter 5.

Table 5. The E-modulus for the 0.001 /s strain rate

	E-Modulus
Average	13.2 GPa
Minimum	9.6 GPa
Maximum	16.6 GPa

The method used to determine the E-modulus followed the same approach as Boshoff (2007) and was used to determine the non-linear initial ascending branch of the stress-strain response. When the response deviates significantly from the linear elastic portion it is assumed that the cracking has developed. In effect there is micro-cracking that develops before the first macro-crack. The cracking gives rise to an initial stress-strain portion with a strong non-linear shape which is more profound with the low loading rates and is shown schematically in Figure 30.

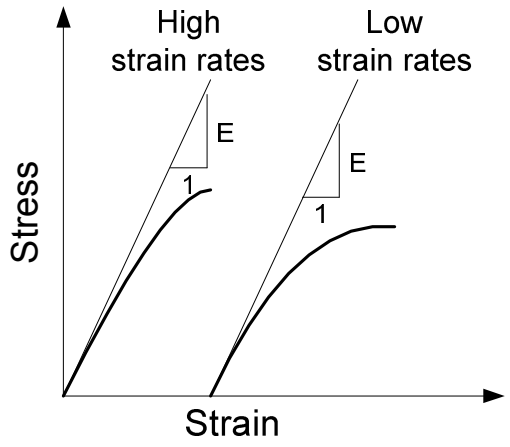

Figure 30. Representation of the non-linear initial ascending branch (Boshoff, 2007)

A linear trend line was fitted to the linear elastic portion of the response for each test specimen from the 0.001 /s strain rate tests to determine the E-modulus. The trend lines had an R-squared value (R^2) of at least 0.975. The gradient of the trend line was determined and the average was calculated for the five test specimens as the E-modulus.

Compression tests were performed on a 2 MN Contest Crushing Machine. Concrete cubes of average 100 mm x 100 mm were used to test the compression strength. The five mixes that were used for the uni-axial tensile tests resulted in an average compression stress of 24.1 MPa at 14 days. The minimum and maximum compression stress values for this SHCC mix was 22.1 MPa and 26.2 MPa respectively. This shows that the five batches had good repeatability.

4.3 Shrinkage and Sustained Tensile Loading Tests

4.3.1 Shrinkage

In order to find the creep strains for the sustained tensile loading tests the shrinkage results were subtracted from the creep strains. The shrinkage strains are shown for a period of 64 days for the four shrinkage test specimens in Figure 31. The shrinkage results start at time zero which is 14 days after the specimens were fabricated. These specimens were exposed to the same climate as described in Figure 14 a) and b).

One of the test specimens gave rise to a deviation after 5.8 days. The shrinkage strains for this specimen were significantly lower than for the three remaining test specimens. This test specimen's shrinkage results were discarded from the average shrinkage strains as this deviation was most probable due to a measuring error. The average shrinkage strains, over the 64 day period, were determined from the remaining three shrinkage test specimens and are shown in Figure 32. Note that the shrinkage strain has been deducted from all the creep strains in this chapter.

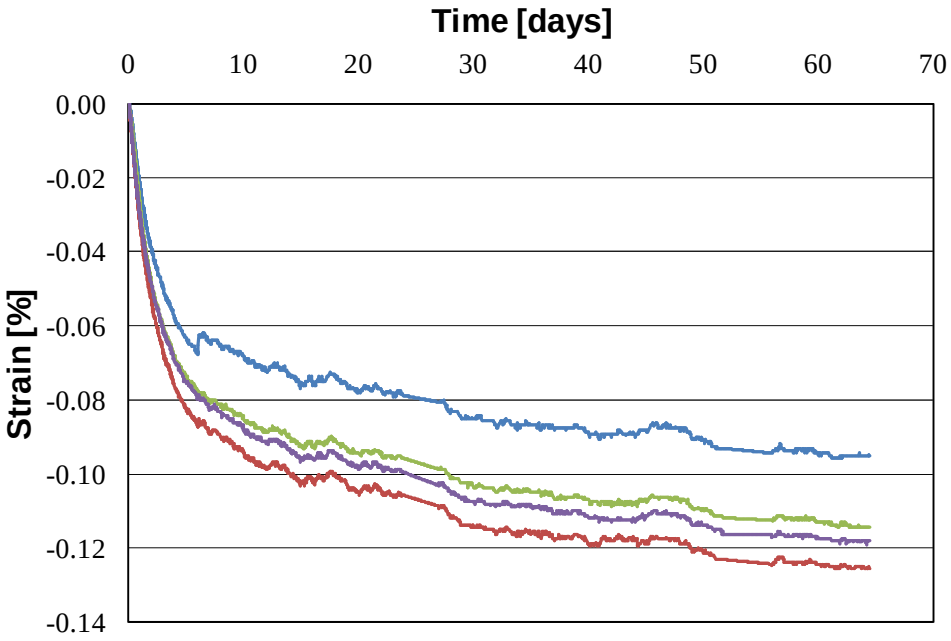

Figure 31. The shrinkage strain readings for the four test specimens

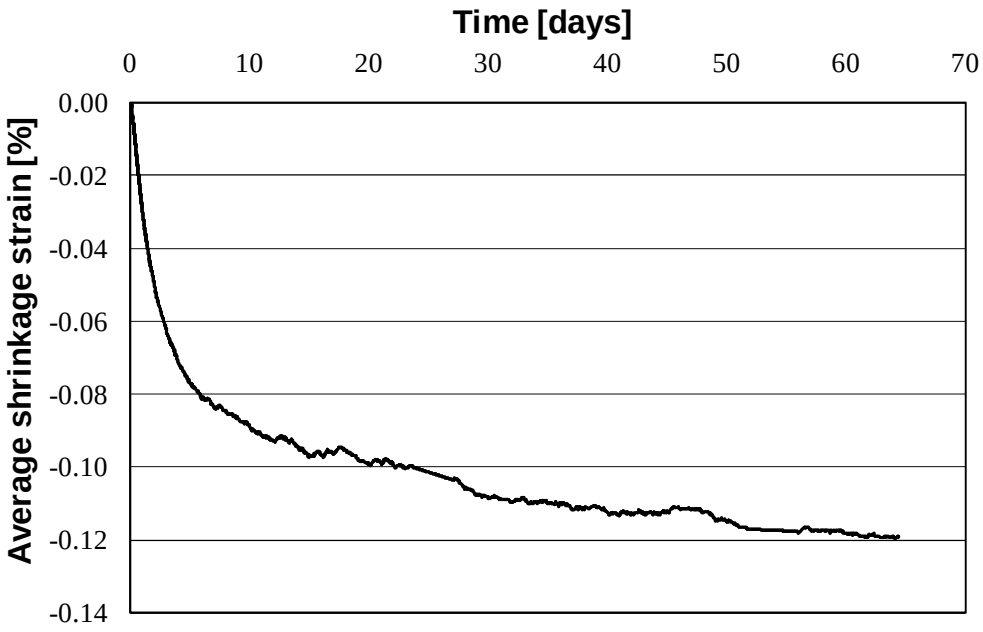

Figure 32. Averaged shrinkage strains for the three specimens

4.3.2 Creep

For clarity the results of the sustained tensile tests are shown in the following manner: The creep results are grouped depending on the time to failure or the loading levels used. These specimens were not used for the crack analysis, since the failure of the specimens occurred within 10 minutes of loading or did not crack in the observed area. In Figure 33 the graphs depict the ten specimens that failed within 1 minute, six specimens that failed between 1 and 10 minutes and creep strains of two specimens, namely A1 Top and A1 Bottom, which did not crack in the observed area. The time is expressed in seconds, minutes and days for the three figures respectively. The black markers indicate the failure of the individual specimens. The corresponding specimen did not fail, however were terminated since the two specimens were in series.

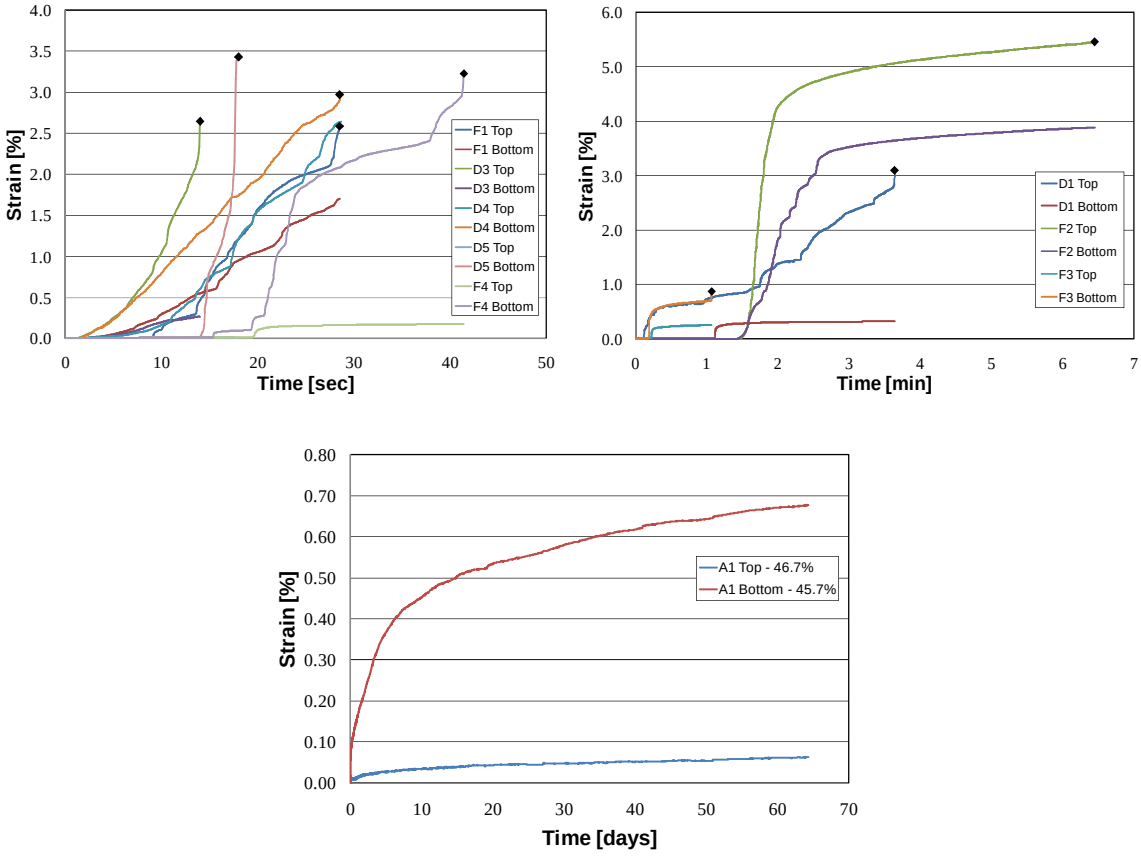

Figure 33. The creep results of the specimens not used for the crack analysis

The twelve specimens that were used for the determination of the time-dependant cracking behaviour are depicted in Figure 34 with their respective creep strain readings. These specimens were loaded between the ranges of 40 % to 80 % of the ultimate resistance tensile stress. Creep fracture occurred for six of the specimens after a certain time which led to the termination of the tests on all twelve test specimens.

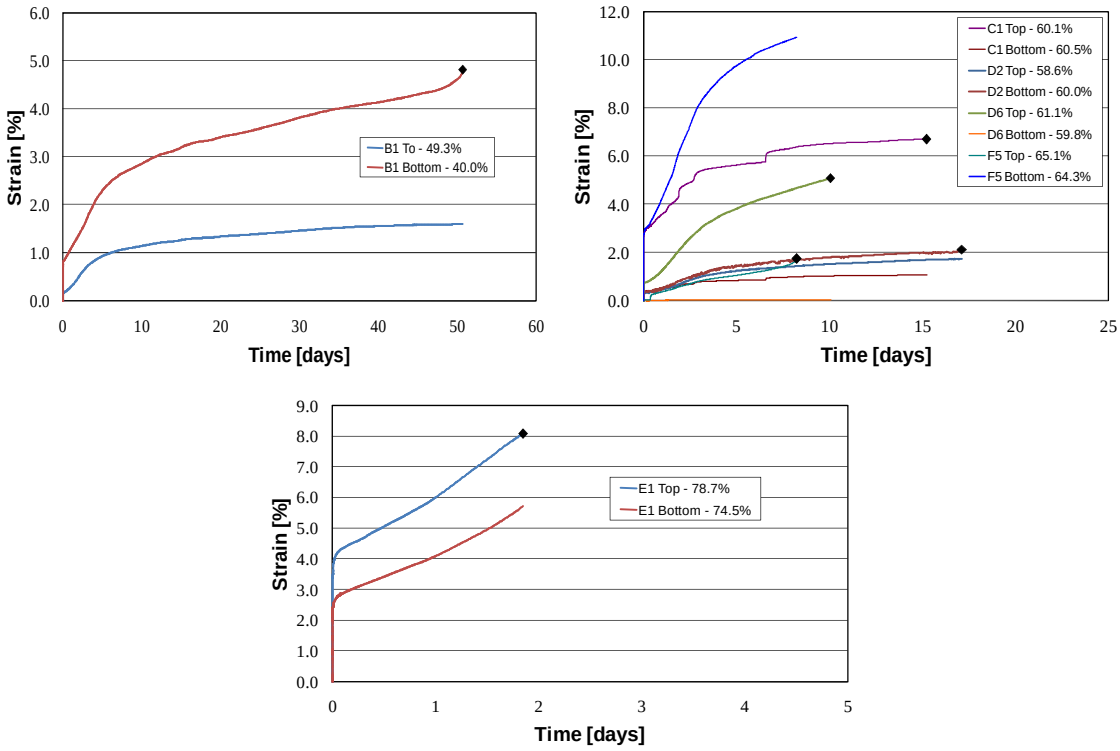

Figure 34. The creep strains for the twelve specimens that were used to determine the cracking behaviour, with loading percentages varying between 40 % and 80 %

The creep compliance was determined using the creep strains for the fourteen specimens that did not fail before 10 minutes. The creep compliance was determined for four time frames. These four time frames are the only time frames in which the fourteen specimens had not failed which added to the reasoning of choosing these specific time frames. The

four time frames for the creep compliance are 1 minute, 5 minutes, 1 day and 1.5 days and are shown in Figure 35.

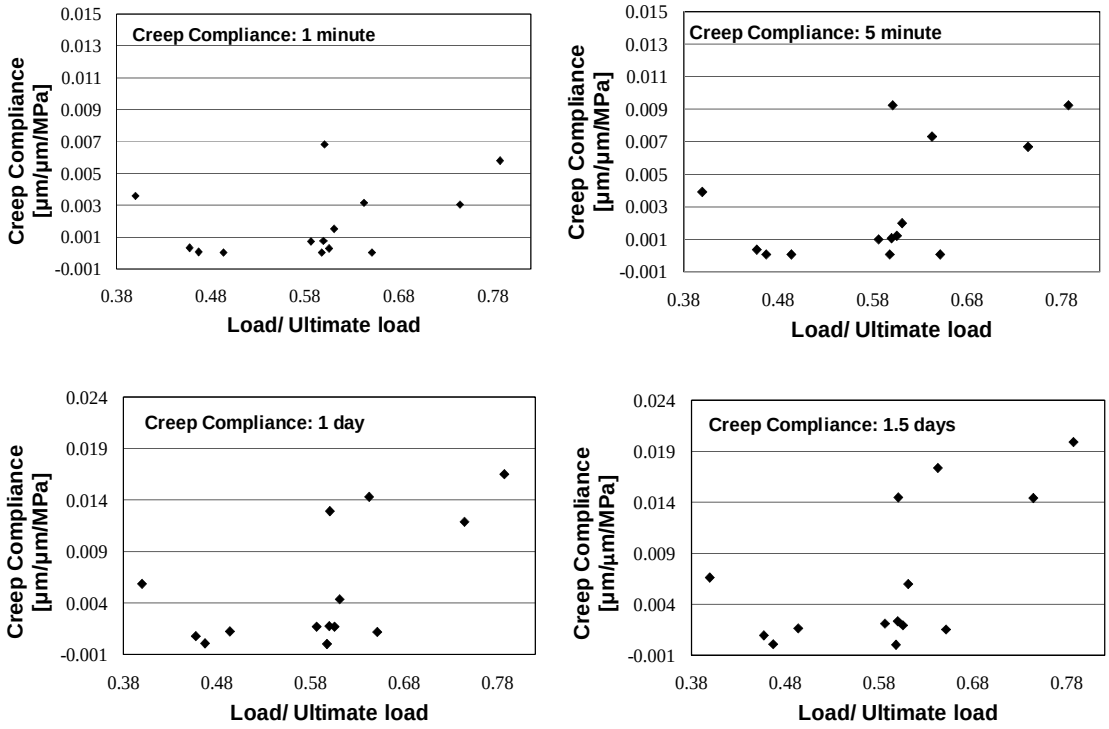

Figure 35. The creep compliance for each load ratio at different time frames

Six of the twelve specimens that were used for the determination of the cracking behaviour fractured after a certain time which led to the termination of their six paired test specimens. In Figure 36 all the creep specimens that were tested are shown with their respective time until failure. The two specimens, namely A1 Top and A1 Bottom are the only two specimens that did not fracture and are not shown in Figure 36.

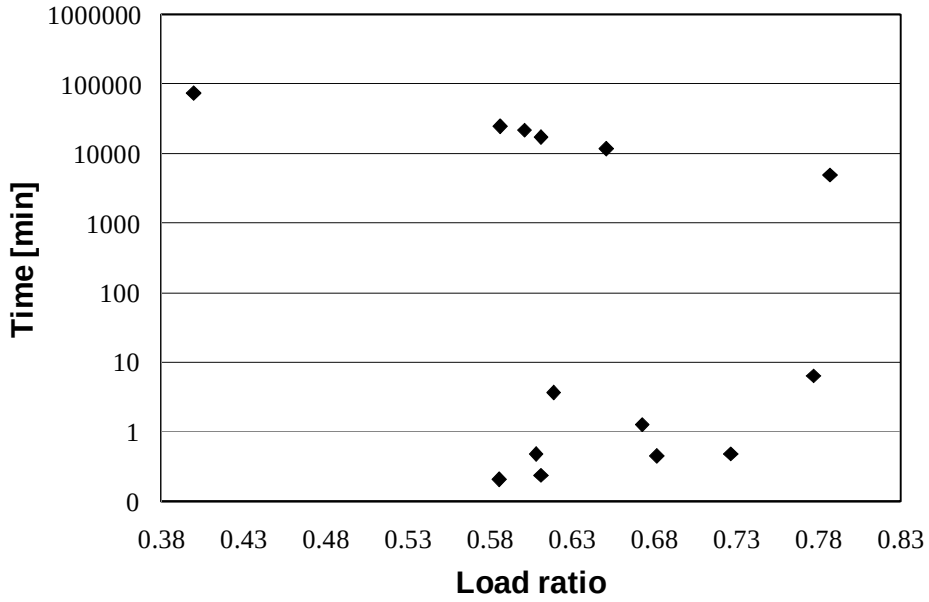

Figure 36. The time to fracture for all the creep specimens

4.4 Discussion

Relative good repeatable results were found for all the rate tests. The coefficient of variance of peak stress for the 0.00001 /s, 0.0001 /s and 0.001 /s strain rates is 9.3 %, 9.4 % and 9.7 % and for the 0.01 /s and 0.1 /s strain rates is 15.6 % and 15.1 % respectively. There was one specimen that was discarded from the determination of the cracking behaviour for the quasi-static tensile tests. However, the specimen was included in the determination of the average ultimate stress and strain.

An increase in the average ultimate stress of 3.3 % from the lowest to the highest loading rate was found. This does not correspond to the increase of 17 % and 90 % that was reported by Boshoff (2007) and Maalej et al. (2005) respectively for their HPFRCC test specimens. Kim et al. (2008) showed that the increase in the ultimate stress from the lowest to the highest loading rate for three different mixes with different fibre volumes was between 10 % and 50 %.

The ultimate strain decreased with an increase in loading rate. The decrease in the ultimate strain is 48.6 % from the lowest to the highest loading rate. This decrease in ultimate strain can be attributed to either the reduction of the width of the cracks or the reduction of the number of cracks. The average compression strength for the cement-based composite was 24.1 MPa and showed reasonable good repetition of results.

The average shrinkage strains at 64 days for this cement-based composite are in the same order of magnitude that Boshoff (2007) determined, although slight lower percentage shrinkage strain after 64 days were recorded. The shrinkage results indicate a typical cement-based material behaviour. The shrinkage strains are dependant on the size of the specimen and the preparation of the specimen before the shrinkage tests were started. The lower shrinkage strains can be attributed partly to the white lime stone layer that was painted on the specimen over the gauge length as well as the compressed air used for the surface drying of the specimen before each test. The duration of the drying process was average 1 minute.

The creep strains are relatively high for the higher loading percentages. Some of the creep strains even exceeded the ultimate strain capacity of the quasi-static tensile tests of the lowest strain rate. The higher strain when loaded with a sustained load can be attributed to either the increase of the widths of the cracks or the number of cracks from what was determined for the quasi-static tensile tests.

The results of the creep compliance do not resemble the expected curve as described in Chapter 2 when the creep compliance is plotted against the corresponding load ratio. A trend line was not fitted for the data since the values of the creep compliance for the different load ratios are significantly scattered. The creep compliance values indicate that for this SHCC the behaviour varies significantly when loaded under different sustained tensile loads and further investigation is needed into the reliability and the creep fracture of SHCC.

Figure 36 clearly shows that specimens that are loaded in the range of 55 % to 80 % of the ultimate tensile stress can be divided into two groups: Specimens that fractured within 10 minutes and specimens that fractured after 6000 min (100 hours). The creep fracture of the

test specimens shows a clear trend of a decrease in time of creep fracture with increase in load. The early fracture of the specimens when loaded at a higher loading percentage can be due to fibre rupture, however the true mechanisms contributing to the fracture of specimens within 10 minutes at loads of higher than 55 % of the ultimate stress as well as the envelope of creep fracture after a certain time period are still unknown.

4.5 Summary

Quasi-static tensile tests were performed using five different strain rates. The main objective of performing the rate tests was to determine what the effect is on the cracking behaviour of SHCC. The different rate tests showed fairly good repetition of stress strain response curves. The material behaviour indicated that the average ultimate stress is reasonably constant at 4 MPa. However, the average ultimate strain decreased with an increase in loading rate from the lowest to the highest strain rate.

This chapter shed some light on the behaviour of SHCC under a sustained tensile load. The loading varied from 40 % to 80 % of the ultimate tensile stress. Shrinkage tests were also performed to determine the behaviour of SHCC with no applied load. The creep strains found for the sustained loads higher than 65 % of the ultimate tensile stress indicate creep strains of up to 10 % which are significantly higher than the ultimate tensile strain capacity under a uni-axial load with a strain rate of 0.001 /s. This may indicate that a different cracking pattern occurs for static and creep tests.

Creep fracture occurred for six specimens that were used for the determination of the cracking behaviour. These specimens were loaded in the range of 40 % to 80 % of the ultimate tensile stress. This clearly shows that SHCC does exhibit creep fracture when loaded in uni-axial tension.

CHAPTER 5

CRACKING BEHAVIOUR

5.1 Introduction

The cracking behaviour is characterised as the average crack width, number of cracks and some descriptive statistical properties. The statistical properties are chosen to represent the distribution of the crack widths at selected strains that can be used in a future research project to develop a numerical model that will simulate the crack distribution of SHCC under different loading conditions.

In this chapter, the cracking behaviour of SHCC for the different loading rates is discussed as well as for the sustained tensile tests. Based on the author's knowledge there is only one publication, namely Boshoff et al. (2008), about the quantification of the time-dependant cracking behaviour of SHCC under a sustained loading. However, the focus of researchers is turning towards the durability aspect of SHCC and in turn the cracking behaviour under a sustained load.

Tests performed by Boshoff (2007) indicated that for a certain embedded fibre length the different loading rates either cause the fibres to rupture or to pull out. The cracking behaviour shown by Lepech & Li (2005) indicated that the spacing of cracks at saturation is 2 to 5 mm. Boshoff et al. (2008) concluded that the cracking behaviour differs for different loading histories and that the developed crack widths is significantly higher for notched specimens when subjected to a sustained load compared to quasi-static tensile tests.

5.2 Crack Pattern Analysis Framework

The following cracking behaviour characteristics were determined: The average crack width, number of cracks per meter, the variance and skewness of the statistical distribution of the crack widths. These four cracking behaviour characteristics are of importance to be able to represent a distribution model of the crack widths and to determine the variability of the distribution of the crack widths when loaded in tension to a certain strain. Two statistical distributions can have the same standard deviation and average, although the one distribution can be skewed right and the other skewed left. Thus the average crack width, number of cracks, the variance and skewness are of importance to represent a distribution of the developed crack widths for each test specimen.

The average and the variance are two basic statistical properties which on their own cannot describe the distribution of a data set, unless the data set fits a normal distribution. The average of a given data set is the measure of the central tendency. The average crack width and variance were determined for each test specimen using Equation 11 and Equation 12 respectively.

$$Average\ \ crack\ \ width\ = \frac{\sum x_i}{N} \qquad \text{Eq. 11}$$

$$Variance\ = \frac{\sum (x_i - \bar{x})^2}{(N-1)} \qquad \text{Eq. 12}$$

The symbols x_i, $\bar{x}$ and N are the value of each data point, the average value of the data set and the total number of data points respectively. The variance is called the second central moment and is used to indicate the statistical dispersion of a given data set. Although the average crack width and the variance do not indicate whether there is a

development of more small, fine cracks or if some of the existing cracks become larger, therefore an alternative statistical property, namely the skewness was introduced to determine the distribution of the crack widths.

The skewness represents the non-symmetry of a distribution. Normal distributions generally have a value of zero for the skewness. When the skewness value is positive the distribution is said to be skewed right or positively skewed. This means that the tail of the distribution is longer to the right side and the peak of the data is more to the left side. When the skewness value is negative the distribution is said to be negatively skewed or skewed left. This means that the left tail of the distribution is longer to the left and the peak of the data is more to the right side. In Figure 37 these two kinds of distributions are shown.

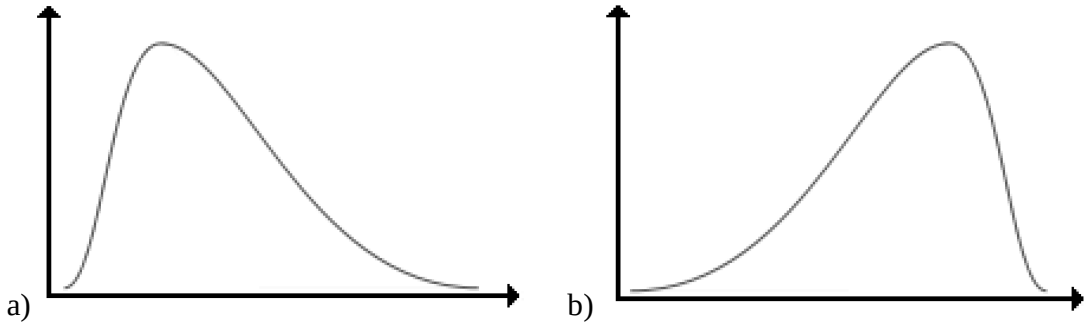

Figure 37. a) A distribution skewed right and b) a distribution skewed left

The skewness can be determined by plotting a histogram of the data set or by mathematical means. The skewness is referred to as the moment coefficient of skewness or the third moment of the data set and is determined with Equation 13.

$$Skewness = \frac{N}{(N-1)(N-2)} \sum_{i=1}^{N} \left(\frac{(x_i - \bar{x})}{s} \right)^3 \qquad \text{Eq. 13}$$

The symbols N, $\bar{x}$, and s are the number of data points, the mean value and the standard deviation of the data set respectively. When interpreting the results of the skewness one can use the rule of thumb suggested by Bulmer (1965) as follows: If the skewness is less than −1 or greater than +1, the distribution is highly skewed. If the skewness is between −1 and -0.5 or between +0.5 and +1, the distribution is moderately skewed and if the skewness is between −0.5 and +0.5, the distribution is approximately symmetric.

The kurtosis describes the peaked or flatness of a distribution for a given data set. The kurtosis is determined with Equation 14. The equation indicates that the kurtosis is determined with terms to the power of 4. The sensitivity of the fourth power gives rise to kurtosis values that are widely spread for each test specimen at corresponding strain values, therefore the kurtosis values were discarded from the cracking behaviour characteristics.

$$Kurtosis = \left\{ \frac{N(N+1)}{(N-1)(N-2)(N-3)} \sum \left(\frac{x_i - \bar{x}}{s} \right)^4 \right\} - \left\{ \frac{3(N-1)^2}{(N-2)(N-3)} \right\} \qquad \text{Eq. 14}$$

At certain areas on the analysed area the coordinates in the deformed state could not be determined by the ARAMIS system due to the stochastic pattern failing. The coordinates in the deformed state that could not be determined were interpolated for the calculation of the crack width. The interpolation was done with the ARAMIS software and used the surrounding coordinates in the deformed state at the area that was interpolated.

The section line, as discussed in Section 3.3, is divided into a number of points. Each of these points is a known distance from each other in the reference stage and the points are referenced with coordinates in the undeformed and deformed state. The displacements of the points in the x and y direction, as shown in Figure 38, were used to determine the distance between the points in the undeformed and deformed state with the Pythagorean Theorem.

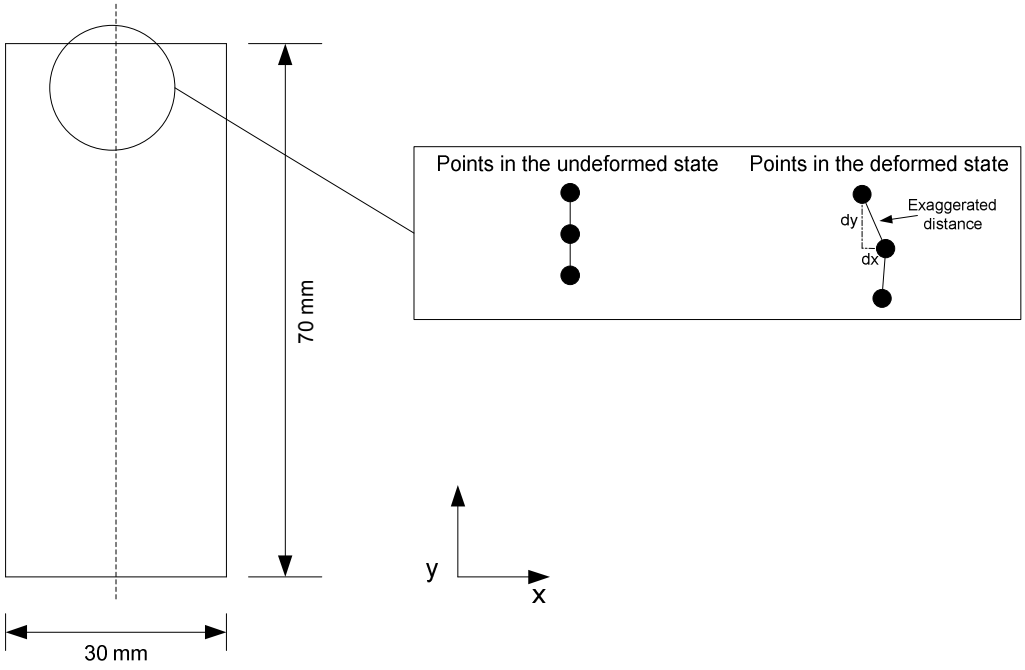

Figure 38. The displacement determined with the shown x and y coordinates system

Due to the micro cracking in the initial ascending branch of the stress-strain response under uni-axial tension the determined local deformations between two points was limited with a lower bound value. For the uni-axial tensile tests a “crack” was declared only after a local deformation on the observed surface area was greater than 10 µm. A test was needed to determine if the lower bound value of 10 µm was appropriate. Therefore, the difference in the displacement between the distance determined with the coordinates in the deformed state relative to the distance determined with the coordinates in the undeformed state was determined with the corresponding stages in the initial ascending branch of the stress-strain response. The results gave rise to positive local deformations between two points of between 0 µm and 10 µm. Therefore, the assumption is valid for the chosen lower bound value of 10 µm. The two sensors that captured the images for the uni-axial quasi-static tensile tests were static for the full duration of the test. However, for the sustained tensile tests the two sensors were moved from the one test specimen to the next while the tests were in progress. The movement of the two sensors gave rise to sporadic local deformations between points determined of between 0 and 15 µm. Therefore, the “crack

width" was limited with a lower bound value of 15 µm for the sustained tensile test specimens.

The difference in displacement between the distance determined with the coordinates in the deformed state relative to the distance determined with the coordinates in the undeformed state is stated as the width of a crack, provided that the local deformation between two points is greater than 10 µm or 15 µm for the respective tests.

A typical crack pattern that was observed for the creep specimens is shown in Figure 39. The three pictures indicate the cracking pattern of the creep specimen F5 Bottom at 1.7 days, 2.7 days and 6.9 days respectively.

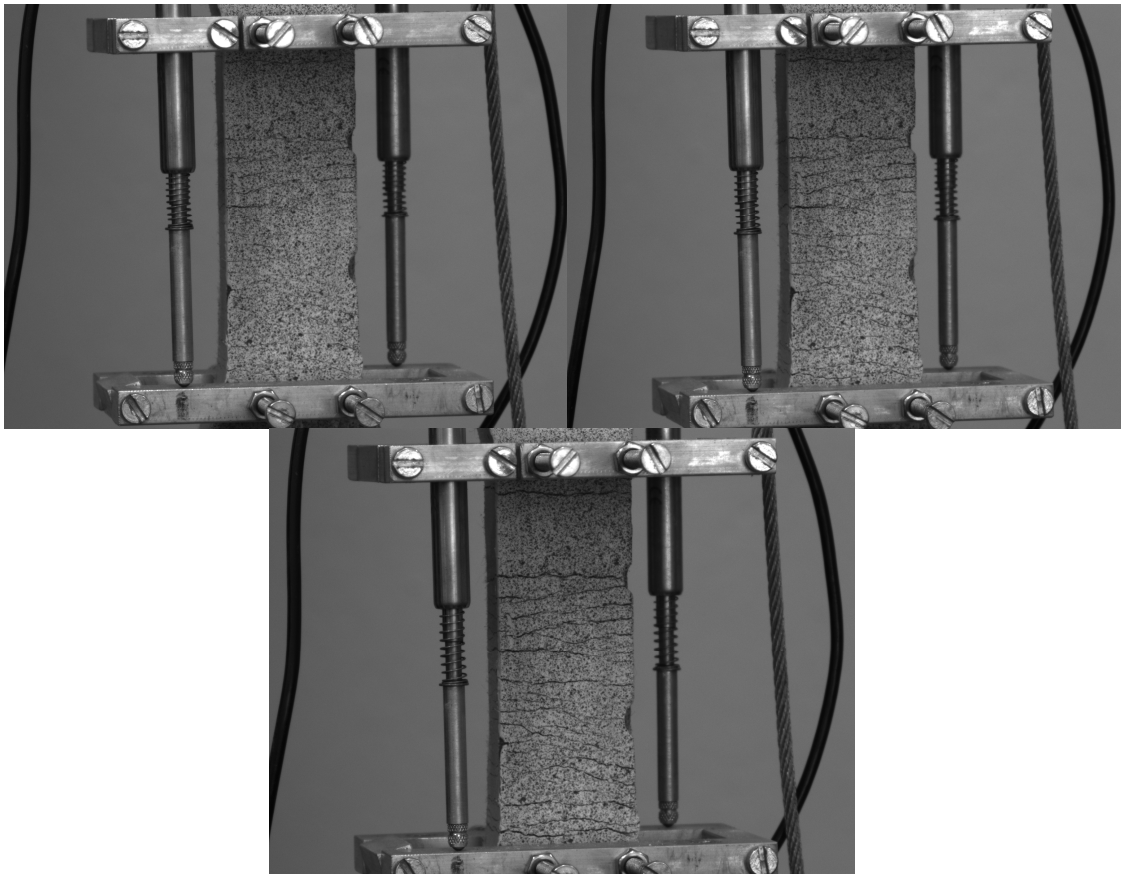

Figure 39. Typical crack pattern observed for a creep test specimen at 1.7 days, 2.7 days and 6.9 days

The local deformation between two points that was determined with the coordinates in the undeformed and deformed state as explained above were used to determine the number of cracks. Thereafter, the crack widths were determined and the average crack width.

The number of cracks multiplied by the average crack width yielded a displacement. This displacement is over a gauge length of 70 mm. The strain values were determined with the displacement over the vertical length of 70 mm for different stages. Thus the strain values represent the cracks that develop over the surface area of 70 mm x 30 mm and not over the volume of 30 mm x 15 mm x 80 mm as recorded with the LVDTs.

The crack width that was calculated with the coordinates in the undeformed and deformed state from the ARAMIS software was verified with an independant computer program. One of the images that were taken with the ARAMIS system for one of the sustained tensile test specimens was imported into CAD, a computer software program, and scaled with a scaling factor to the correct dimensions. The crack width was measured with a tool in the CAD software. The result of the measured crack width was compared to the crack width determined with the ARAMIS software. The values are shown in Table 6.

Table 6. Crack width determined with the ARAMIS system and the CAD software

	Creep specimen	Stage number	Crack width [µm]
ARAMIS System	B1 Bottom	165	969.3
CAD Software program	B1 Bottom	165	1034.9

The variation in the value determined from the CAD software is ascribed to the inaccurate measuring procedure. In Figure 40 a) an image of the specimen with the developed cracks is shown and Figure 40 c) was used to determine the width of the crack in the CAD software.

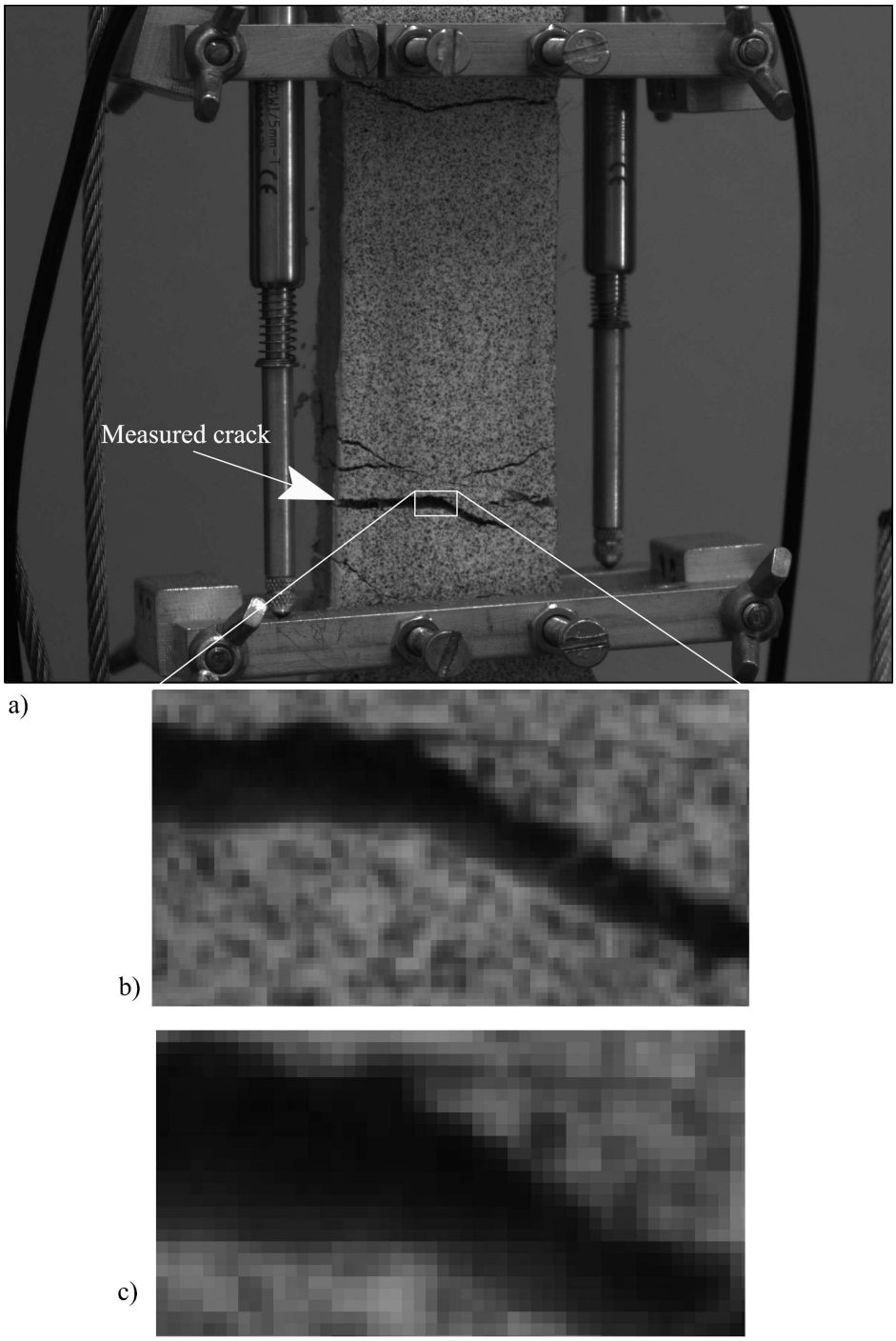

Figure 40. a) The test specimen shown with the developed cracks and the maximum crack that was measured in the CAD software, b) Enlarged view of the measured crack, c) Even more enlarged view of crack

The same crack that was determined in ARAMIS as the maximum crack was measured in the CAD software. Two points opposite each other on the edges of the discontinuity in the middle of the test specimen were measured. The low quality of the image restricted the ability to obtain an objective point on the edges of the surface discontinuity which results in the measured crack width to be subjective. Thus the measuring technique is not appropriate to acquire the correct width of the cracks, however it is considered to be a fair test to indicate that the maximum crack width determined by ARAMIS is in the correct range.

5.3 Quasi-static Cracking Behaviour

The corresponding stress values for the determined strain values over the length of 70 mm are plotted for the different strain rates in Figure 41. Note that the one specimen that was discarded from the 0.001 /s strain rate tests is not included in the graph. The strain levels at which crack widths were determined were chosen at 0.3 %, 0.6 % and 1.0 % to 4.5 % with 0.5 % increments.

Figure 42 to Figure 45 depict the average crack width, variance, number of cracks per meter and the skewness of the statistical distribution of the crack widths at the selected strain values. The cracking behaviour was determined for the developed cracks over the gauge length and it must be kept in mind that the gauge length for the cracking behaviour is 70 mm and not 80 mm as measured with the LVDTs. The cracking behaviour describes the two dimensional cracking pattern on the face of the test specimen. The number of cracks that developed over the 70 mm length is normalised to give a number of cracks per meter at the selected strain levels. The average of the average crack width, number of cracks, the variance and skewness of the distribution of the crack widths at the selected strain values are determined for each strain rate test and are shown in red on the graphs. The one specimen that was discarded from the 0.001 /s strain rate tests is shown in blue. The specimen was discarded on the bases that the average crack width rendered values of more than two times the standard deviation plus the average for the first few selected strains. The variability found for the statistical skewness distribution of the crack widths for each test

specimen at the selected strain values is ascribed to the high sensitivity of the determination of the skewness as the terms are to the power of 3.

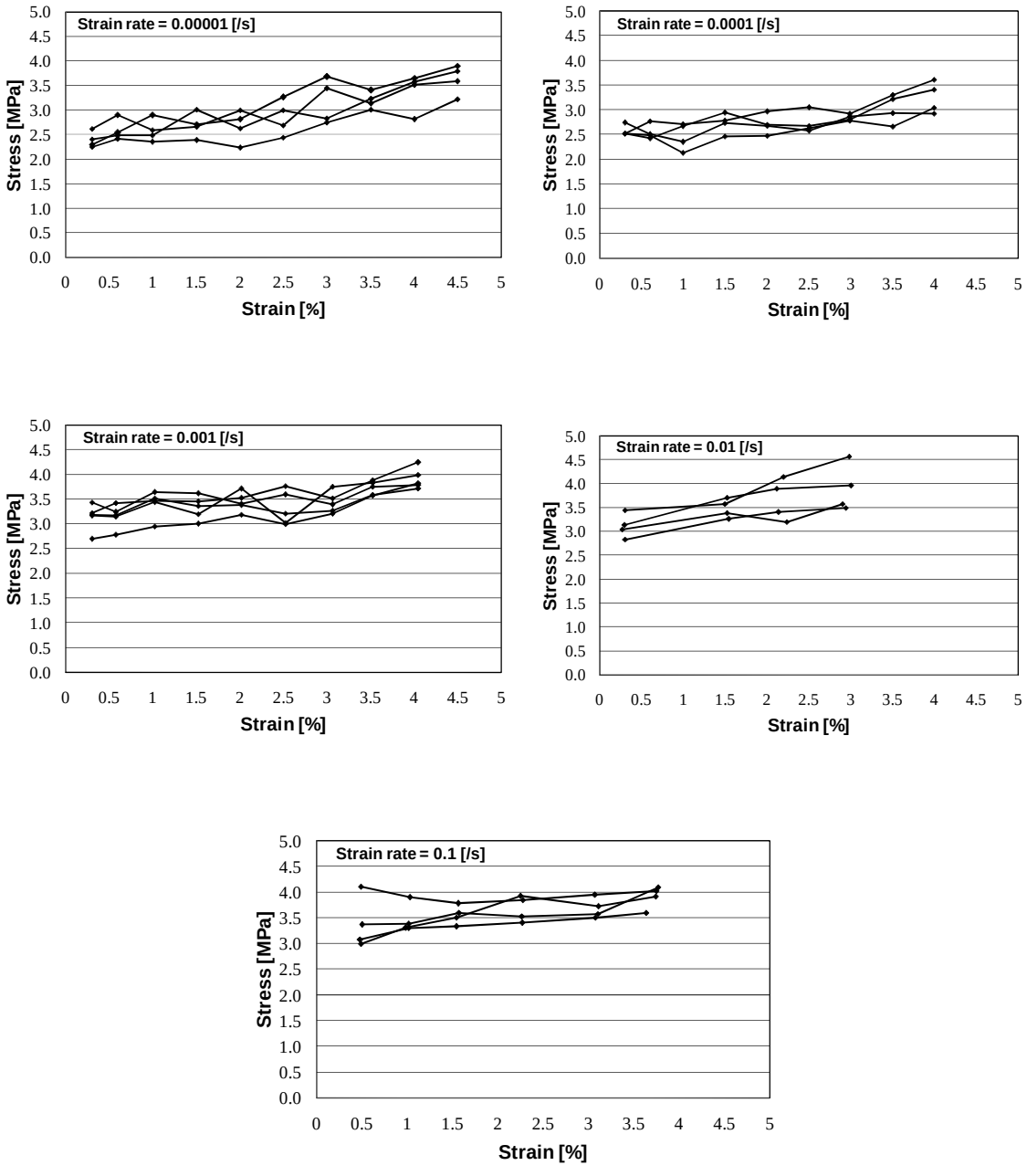

Figure 41. The chosen strain values with the corresponding stress values for the different strain rates

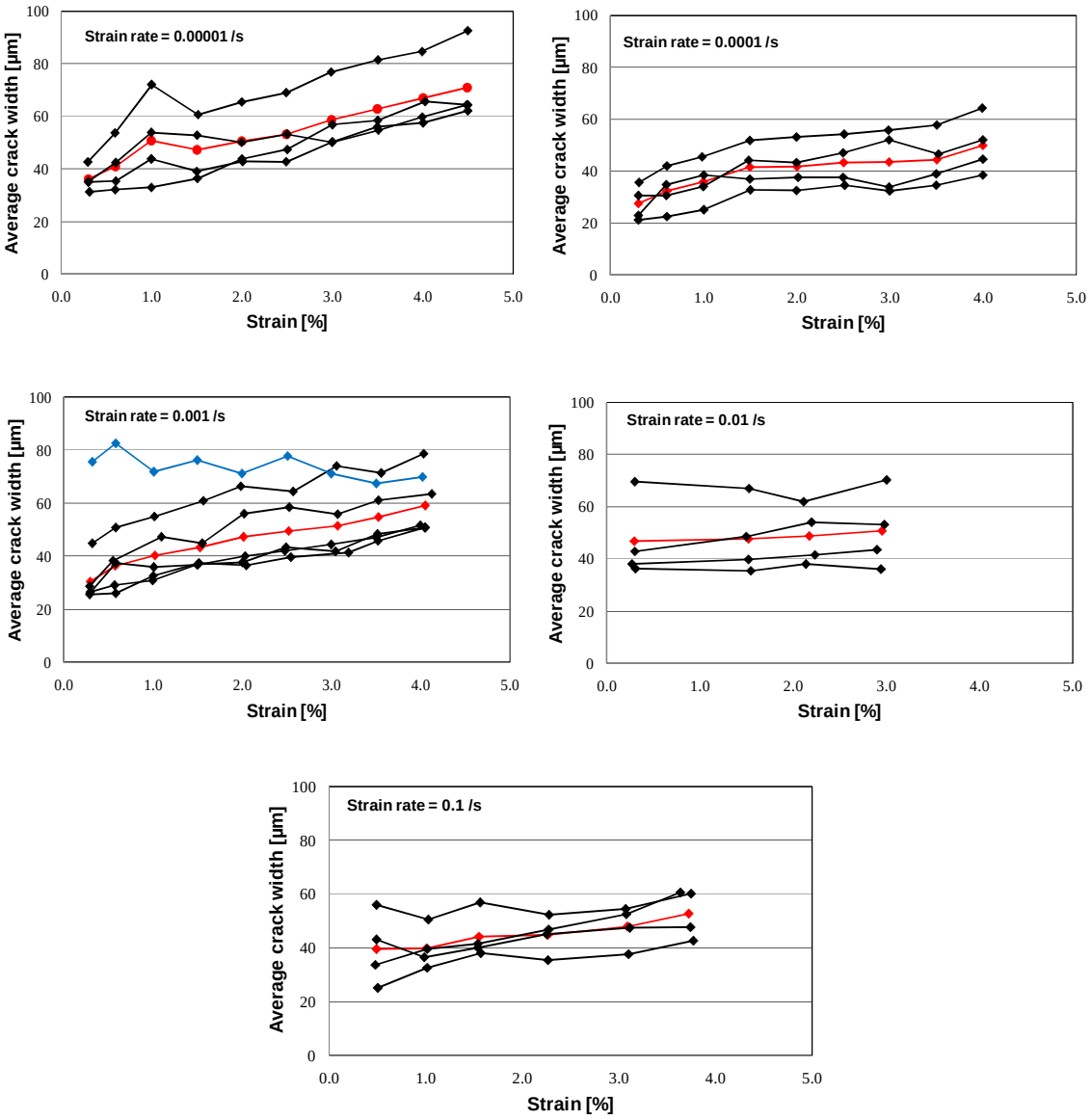

Figure 42. The average crack width for each test specimen for each strain rate

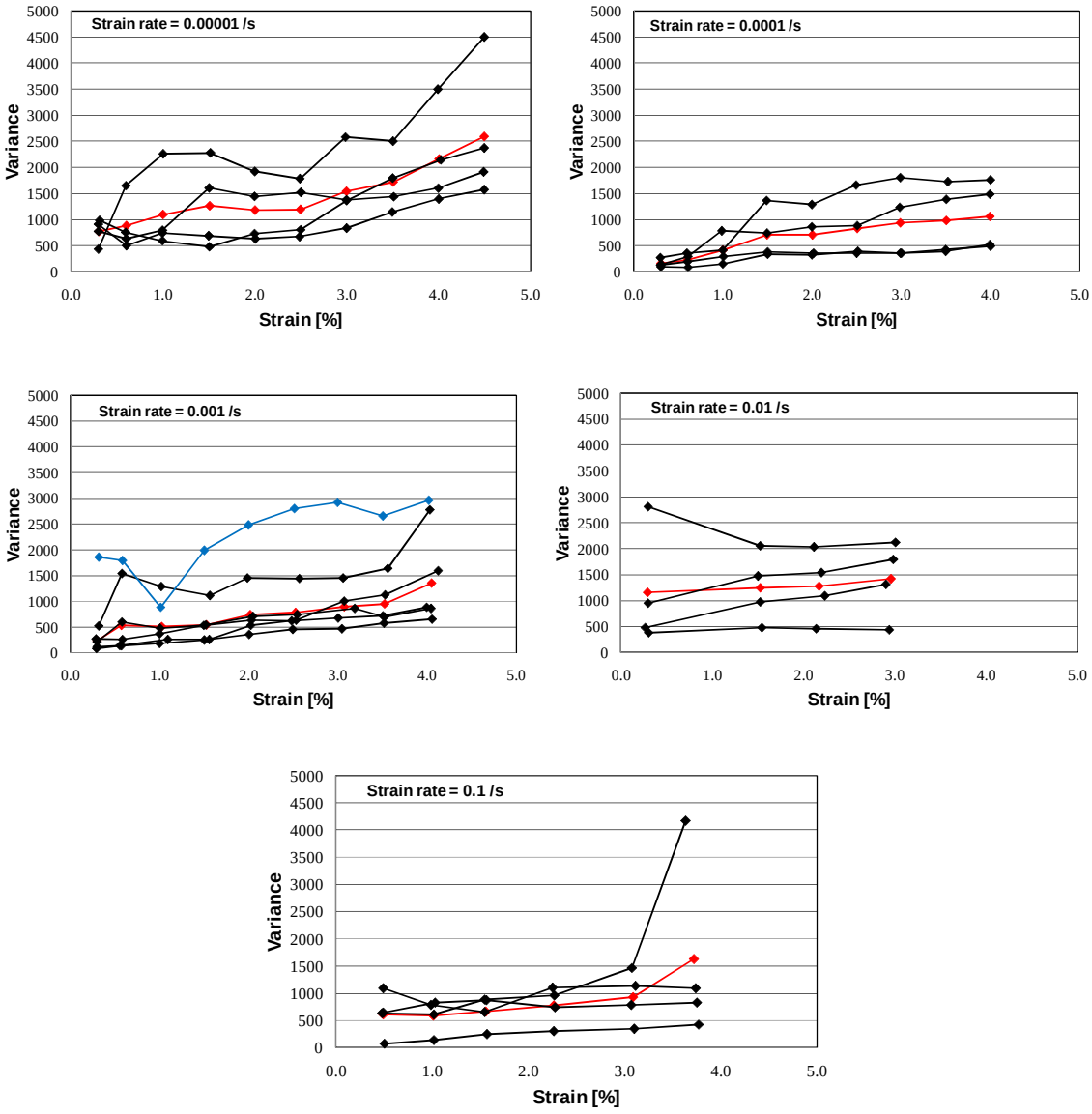

Figure 43. The variance of the crack width distribution for each test specimen for each strain rate

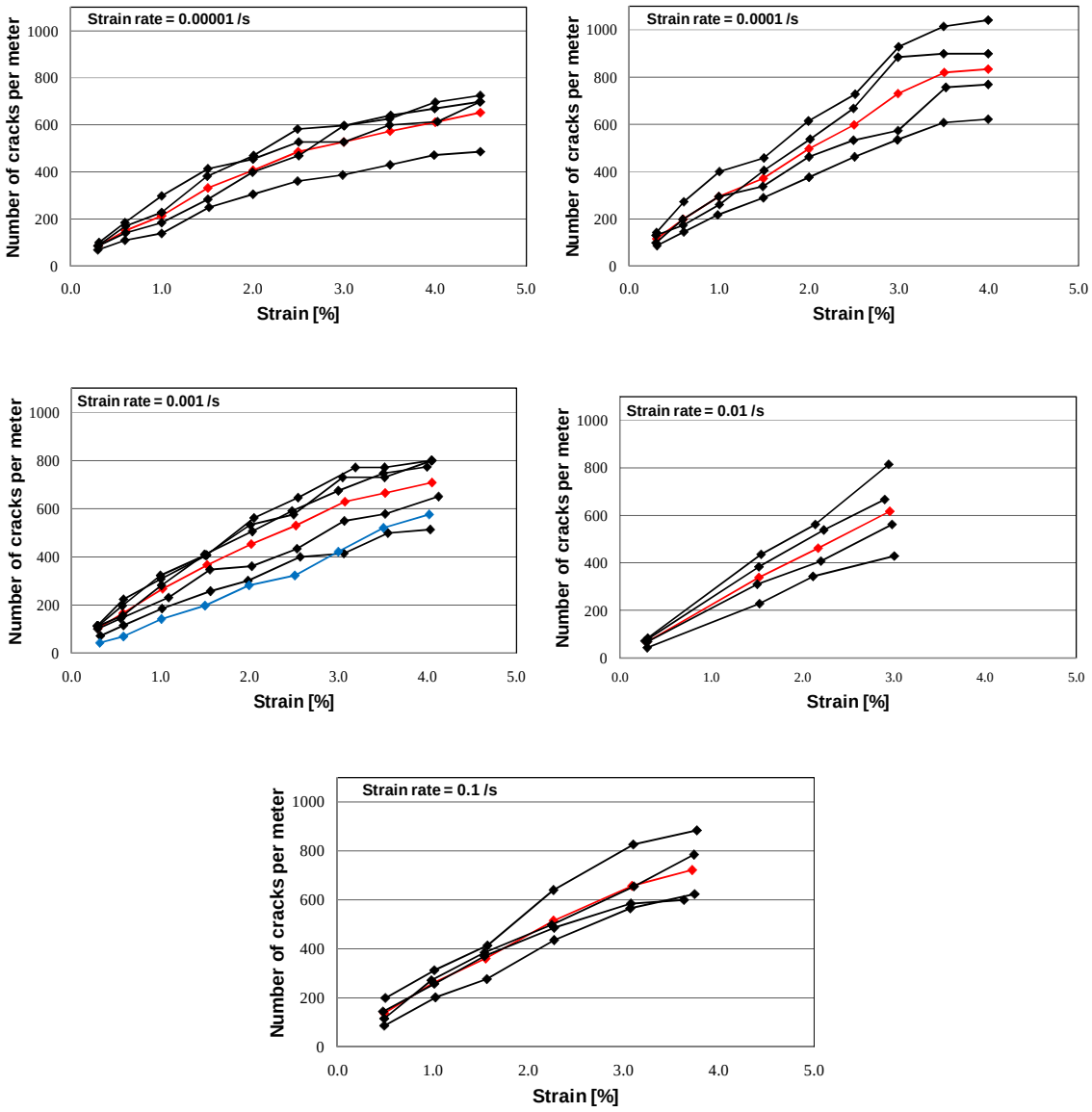

Figure 44. The number of cracks for each test specimen for each strain rate

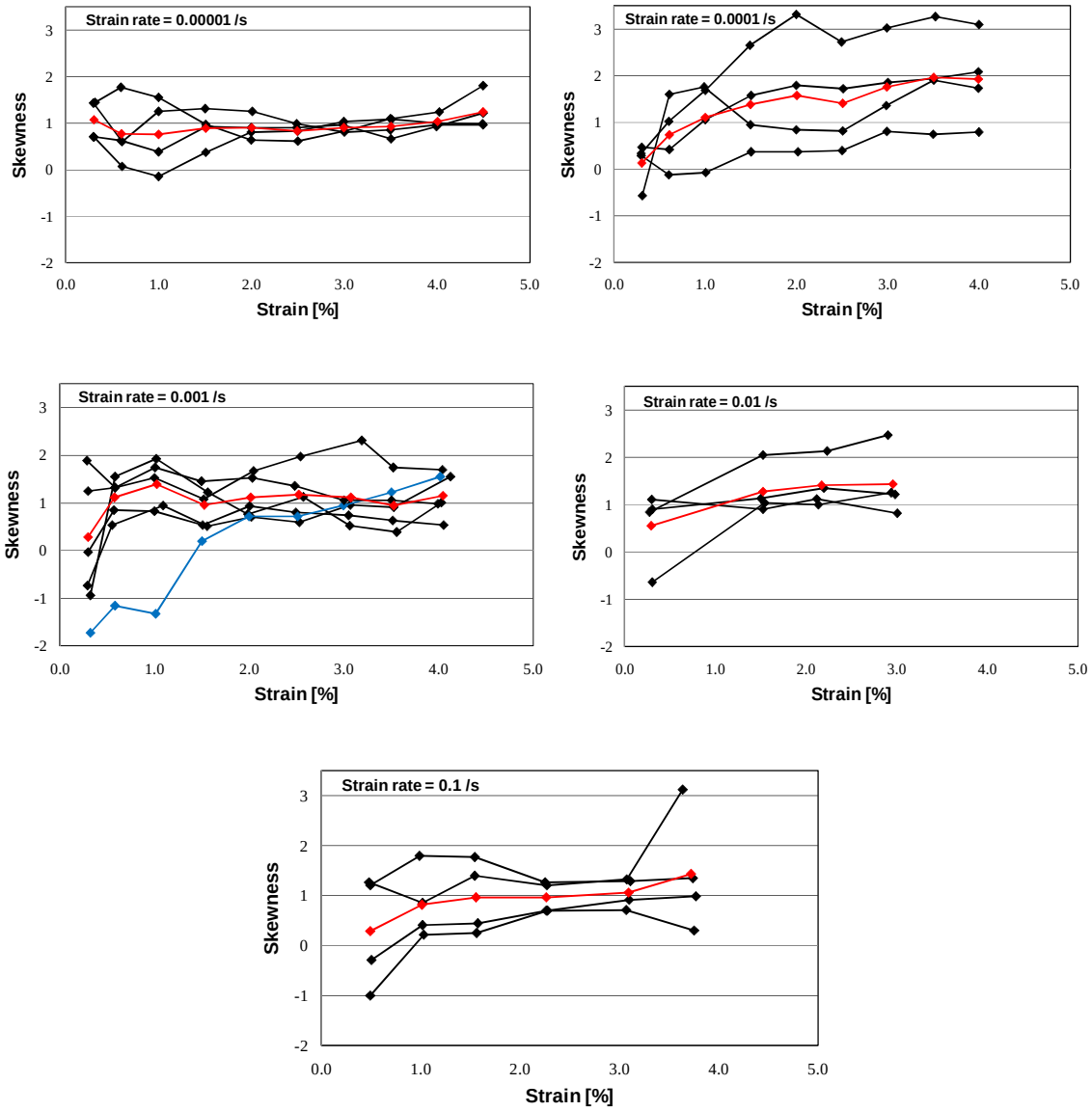

Figure 45. The skewness of the crack width distribution for each test specimen for each strain rate

The average of the average crack width, number of cracks per meter, the variance and skewness of the distribution of the crack widths for the selected strain levels for each strain rate are shown in Figure 46.

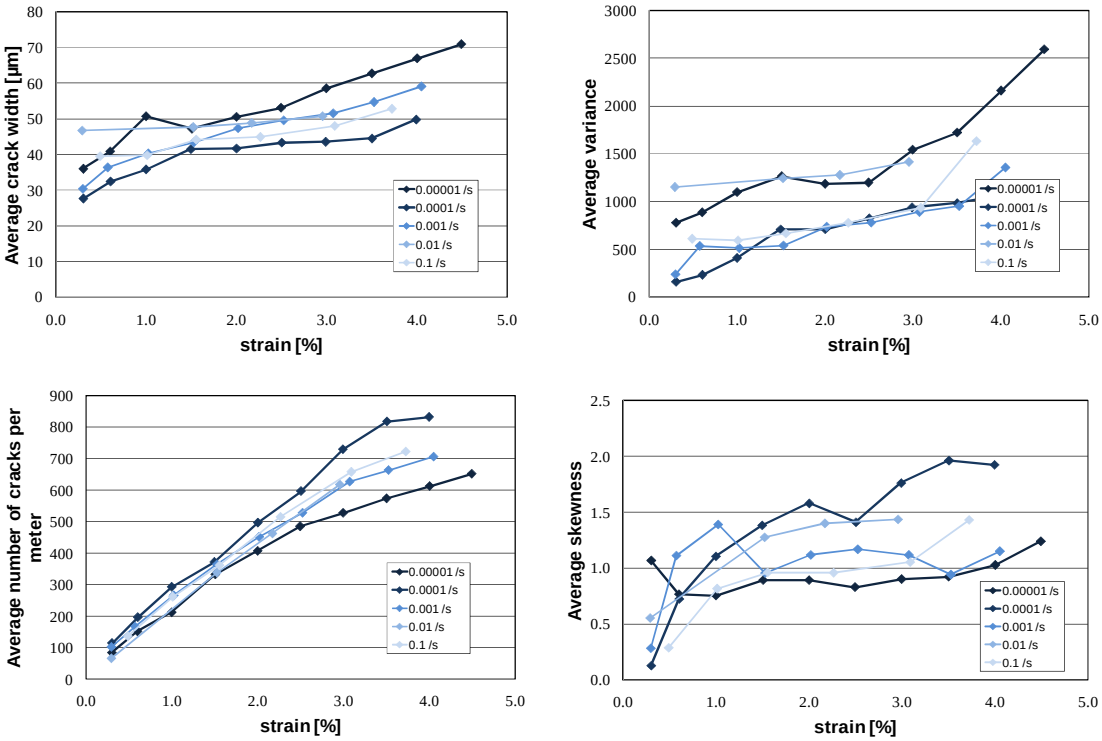

Figure 46. The average of the cracking behaviour characteristics for the different loading rates

The average of the average crack width and of the number of cracks per meter for each strain rate at strains of 1 %, 2 % and 3 % are indicated in Figure 47.

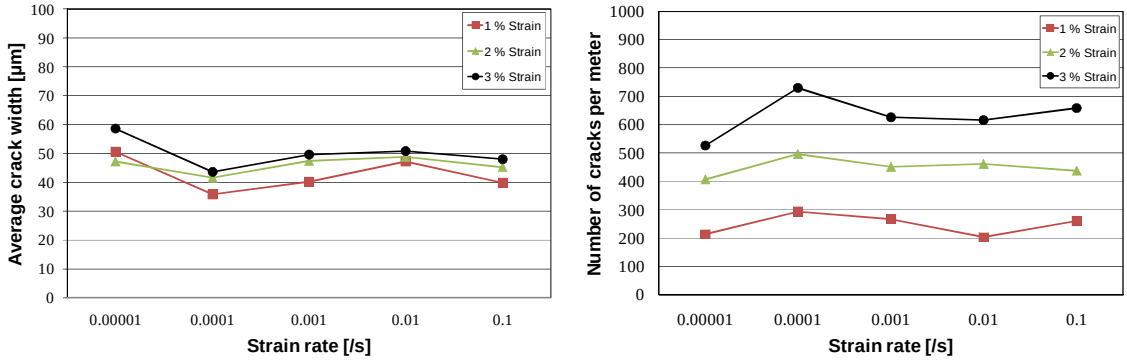

Figure 47. The average crack width and number of cracks per meter for selected strains

5.4 Sustained Loading Cracking Behaviour

Twelve specimens were used to determine the time-dependant cracking behaviour of SHCC. However, two specimens' cracking behaviour, namely D2 Bottom and D6 Bottom, could not be determined, since there was no crack development in the observed area and therefore the ARAMIS software could not be used to determine the cracking behaviour, although the one specimen, D2 Bottom, showed a creep strain of up to 2 %. The reason for this is that the cracks developed outside the ARAMIS gauge length of 70 mm, however within the gauge area measured by the LVDTs. Therefore only ten specimens were used to determine the cracking behaviour for the sustained loading tests.

The characteristics of the cracking behaviour are given in graphical format for easier representation. The average crack width, number of cracks per meter, the variance and skewness of the distribution of the crack widths for each test specimen are plotted against the corresponding time frame. Figure 48 to Figure 51 depict the cracking behaviour obtained for the ten specimens. The specimens' data are plotted on three graphs and are grouped by the respective low, medium and high loading percentages.

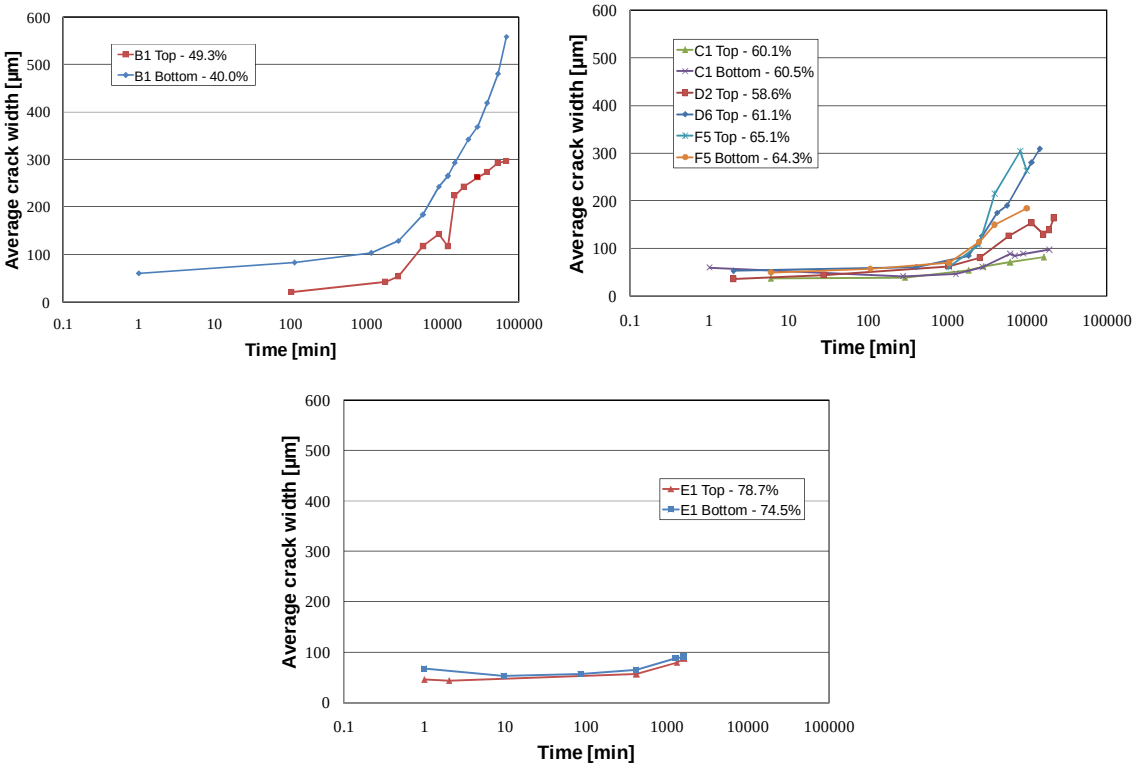

Figure 48. The average crack width for the ten specimens

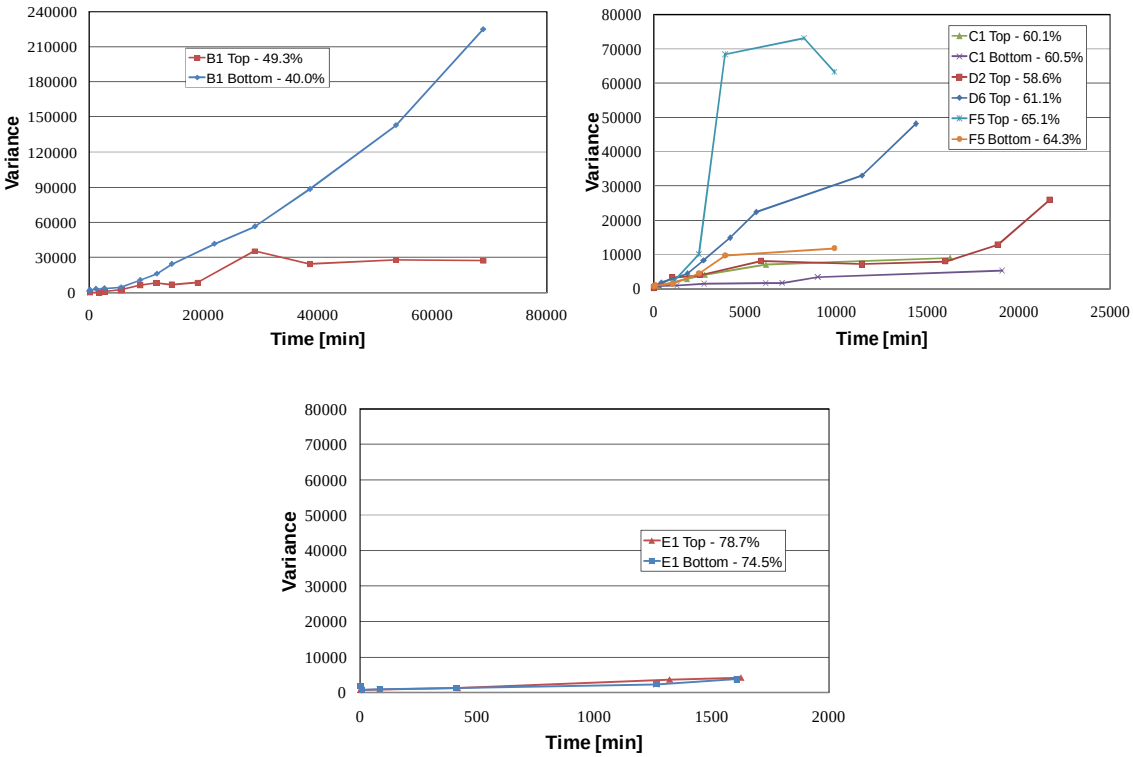

Figure 49. The variance of the crack width distribution for the ten specimens

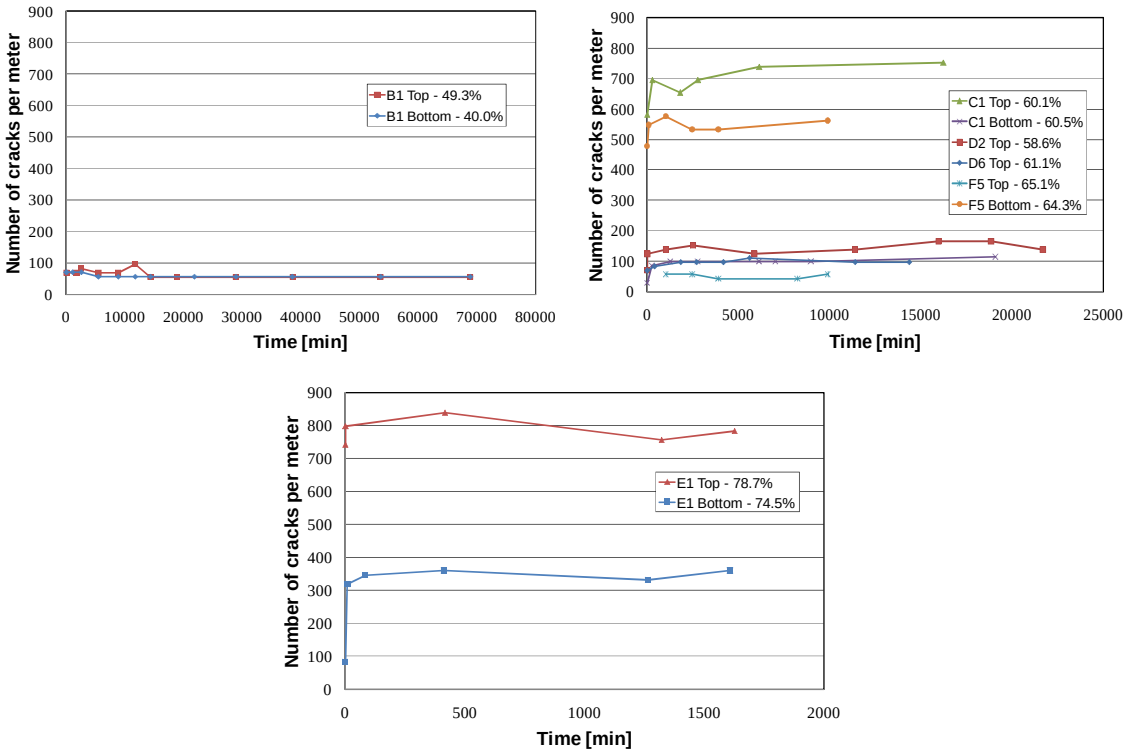

Figure 50. The number of cracks for the ten specimens

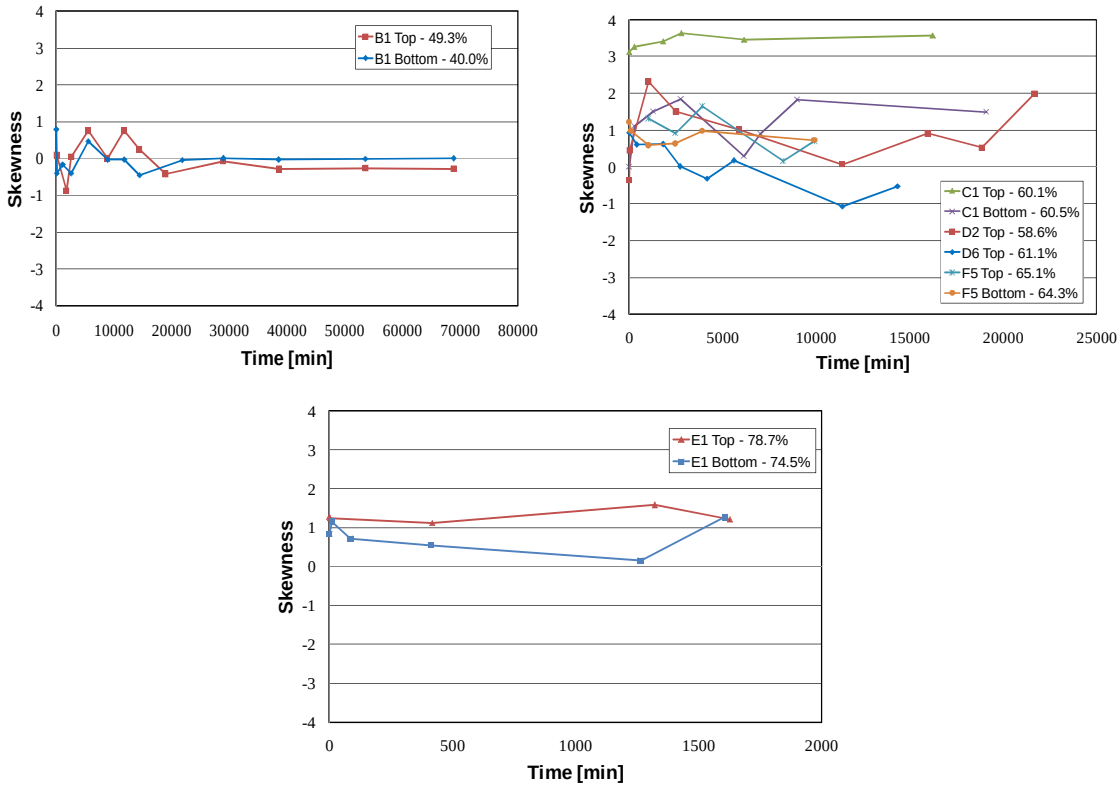

Figure 51. The skewness of the distribution of the crack widths for the ten specimens

5.5 Discussion

The crack widths determined for the five loading rates indicate that the average crack width is smaller than 100 µm at strains up to 4 %. The average crack widths as well as the number of cracks show no significant sensitivity to an increase in loading rate as seen in Figure 47. The average crack width determined at a strain of 4 % indicates a decrease from the lowest to highest loading rate of 16 µm or 23.5 %. This decrease in crack width coincides with the mentioned decrease in ultimate strain from the lowest to highest loading rate. Therefore, the reduction of strain capacity at higher strain rates can be attributed to the reduction of crack widths. The increase in the average crack width with respect to the increase in strain for the five different loading rates is shown in Figure 42 with the red lines to be linear, however, with different gradients for each loading rate.

The number of cracks resembles a linear increase until a strain of average 3 % is reached after which the gradient decreases. A stabilisation of the number of cracks occurs at this point which indicates that the specimens reached a semi-saturation point. This point is called a semi-saturation point as cracking still occurs after this point, however at a much lower rate with regard to the strain increase. The test specimen, after this semi-saturation point, either fails suddenly by the widening of a crack or multiple cracks, since the rate of increase of the average crack width remains linear after this semi-saturation point and does not change significantly.

A comparison between the average of the average crack width and the average number of cracks at strains of 1 %, 2 % and 3 % for the five loading rates were made. The crack width does not contribute significantly to the increase from 1 % to 3 % strain, since the average crack width increases with 15 µm from 1 % to 3 % with respect to each loading rate. However, the average number of cracks increases significantly from 1 % to 3 % strain.

The variance and skewness are two descriptive statistical properties which are used to describe the distribution of the crack widths. The average skewness determined for the five different loading rates are positive which coincides with the forming of new fine cracks. The distribution is skewed right which indicates that there are new cracks forming and that the existing cracks widths do not increase significantly enough to alter the distribution. At higher strains an increase in the variance is observed. The variance on its own is difficult to interpret, since the variance describes the statistical dispersion of the crack widths. However, if a low variance is found then all the data points tend to be close to the average crack width and if a high variance is found then the data points tend to be spread out relative to the average crack width. This increase of variance is thus an indication of the increase of the spread of crack widths.

It can be observed that the average crack width varies significantly with regard to the different sustained loads. This variability found in the average crack width for the different sustained loads coincides with the variability found with the creep compliance which indicates that this SHCC has a high variability when loaded with a sustained load. The fibres as well as the fibre/matrix contribute to the strain that develop in this SHCC which contribute to the variability of the average crack width, since the average crack width and

the total number of cracks that develop in the test specimens are a function of the sustained load applied.

The average crack width for all the specimens is below 300 µm, however for the one specimen, B1 Bottom, the average crack width is above 300 µm. The average crack width shows a significant increase after 1000 minutes and this increase gives rise to the failure of the individual specimens. On the specimens with a lower average crack width the formation of more cracks was observed. After a certain time period the number of cracks does not increase significantly and can be said to have reached a stabilisation point. The stabilisation of the number of cracks for the lower and medium loading percentages is clearly not due to the saturation of the test specimen over the gauge length, which is the case when loaded with different quasi-static loading rates. Therefore, the fibre/matrix interface, when loaded with a sustained loading percentage, has a significant role on the cracking behaviour. Thus, the creep of the fibres is crucial and should be investigated. Note that the creep of the fibres and the fibre/matrix interface is inter-dependant. Therefore, the average crack width is a function of the number of cracks that develop as well as the sustained load applied which in turn can be related to the behaviour of the fibres.

The two specimens B1 Top and B1 Bottom with reference to Figure 48 and Figure 50 show that the average crack width increases and the number of cracks stay constant. The stabilisation of the composite in terms of crack development has occurred at the specific stress level and therefore the fibres that are bridging the stress over the crack plane are in a state of creep. The same mechanism is observed for specimen F5 Bottom. More cracks developed in the beginning which stabilises after a certain time which coincides with an average crack width smaller than 200 µm. The crack widening contributes to the failure of the specimens after the stabilisation point is reached for the given stress level.

Specimens B1 Top and B1 Bottom which are loaded at the lowest loading percentage indicate a skewness of zero. However, the skewness value increases toward 1.0 for specimens loaded at higher sustained loads. This coincides with a cracking behaviour that has a distribution skewed right. The variance indicates that at lower sustained loads the distribution tends to be spread out which can be seen by the small number of cracks that form and the larger average crack width when loaded at the lowest sustained load.

In Figure 52 the average crack width, number of cracks and skewness at an average strain of 1 % are shown. Two conclusions can be drawn from these two graphs. Firstly, the cracking behaviour characteristics are different under different loading conditions. The average crack width is significantly smaller corresponding with much more cracks that develop for the quasi-static tensile tests and the average crack width is significantly higher with less cracks developing for the sustained tensile tests. Secondly, the distribution of the crack widths is mainly governed by a skewed distribution for both the quasi-static and sustained tensile tests. However, for the lower loading percentages of the sustained tensile tests the distribution of the crack widths is governed by a normal distribution.

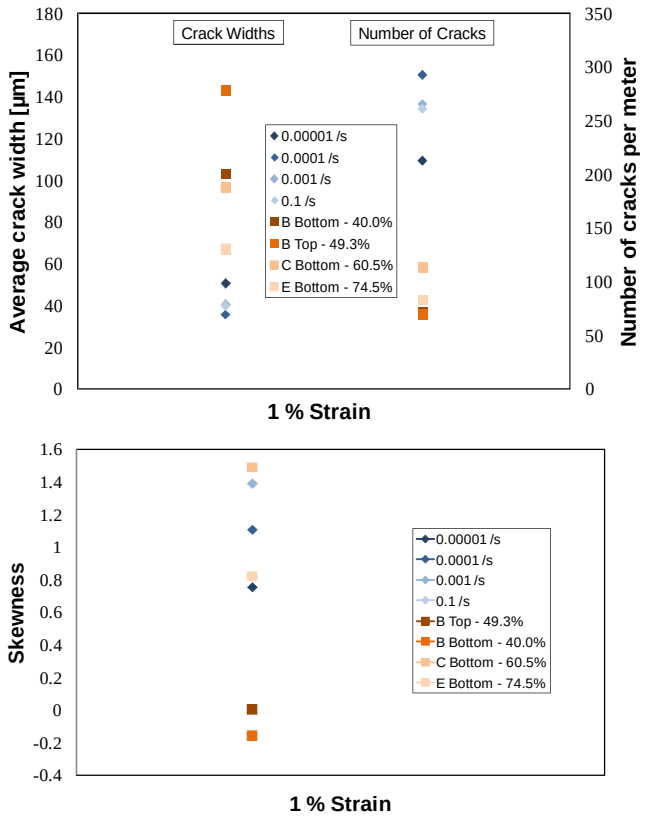

Figure 52. Comparison of the two types of tensile tests with regard to the cracking behaviour characteristics

5.6 Summary

In this chapter a test was performed in order to establish if the determined crack widths from the ARAMIS software are correct. This test indicated that the crack widths determined using the proposed method is accurate.

The cracking behaviour consists of the average crack width, number of cracks, variance and skewness distribution of the crack widths. The governing cracking behaviour is the increase in the number of cracks and not the crack width for the quasi-static tensile tests. The average crack width increases with an average of 15 µm from a strain of 1 % to 3 %. The cracking behaviour indicated that when the test specimens are loaded with a sustained load the average crack width is smaller than 300 µm, however with the exception of one specimen loaded at 40 % of the ultimate tensile stress where the average crack width was larger than 300 µm. This unexpected phenomenon is confirmed by the skewed distribution of the crack widths at higher sustained loads.

The quasi-static and sustained tensile tests shed light on crucial information about the cracking behaviour of SHCC. The different strain rate tests indicated that there is no significant effect on the cracking behaviour, however for the sustained tensile tests the average crack width is dependant on the number of cracks forming as well as the sustained load applied.

CHAPTER 6

CONCLUSIONS AND FUTURE DEVELOPMENTS

6.1 Conclusions

The main objective of this research project was to quantify the cracking behaviour of SHCC under different loading regimes. Uni-axial quasi-static tensile tests as well as sustained tensile tests were performed in order to determine the cracking behaviour characteristics of SHCC under these loading paths in tension. The strain rate tests were varied over five orders of magnitude and the sustained tensile load ranged from 40 % to 80 % of the ultimate tensile stress.

The cracking behaviour characteristics were expressed in terms of skewed normal distribution variables, namely the average crack width, number of cracks per meter, the variance and skewness of the distribution of the crack widths. These characteristics that describe the distribution of the developed crack widths could be used in a future research project to create a numerical model that can simulate and predict the crack distribution for different structural elements.

The two types of tensile tests performed on this SHCC indicated that there is a significant variability in the performance of SHCC under tension. The rate effect on this SHCC indicated a strong influence on the ultimate tensile strain. However, no significant influence was observed for the ultimate tensile stress. The ultimate tensile strain decreased with increase of strain rate and was attributed to the decrease in the crack widths. Some of the test specimens that were used for the sustained tensile loading tests achieved a strain of more than 10 % which is significantly higher than what was achieved with the quasi-static tensile tests for the lowest strain rate. The linear and non-linear behaviour under a sustained tensile load was determined and found that there is a significant variability when loaded with a sustained tensile load. Some of the test specimens achieved a strain of 4 %, 10 %

and 8 % at a sustained load of 40 %, 65 % and 75 % of the ultimate tensile stress before creep fracture occurred. Failure either occurred within 10 minutes for the individual test specimens with a sustained load of 55 % of the ultimate tensile stress and higher, or when loaded with a sustained load of 40 % to 80 % of the ultimate tensile stress failure occurred after 6000 min (100 hours) which resulted in the creep fracture of the individual specimens.

There was no significant effect found on the average crack width and the number of cracks with respect to the different strain rates. The increase in strain during a quasi-static tensile test was characterised by the development of new cracks rather than by the increase in crack width. The increase in the average crack width is on average 15 µm from 1 % to 3 % tensile strain, however the increase in the number of cracks is significantly higher. During a test the increase in the average crack width can be represented by a linear model. However, the increase in the number of cracks can be represented by a bi-linear model. The number of cracks increases until a certain semi-saturation point is reached followed with a slight decrease in the rate of new developed cracks. A conclusion is made that the failure of the test specimens is due to the saturation in terms of the number of cracks which leads to the sudden increase in crack width for either a crack or multiple cracks. This failure can be attributed either to the rupture or pull-out of fibres or both. The skewness of the distribution of the crack widths with increase in strain during a quasi-static tensile test indicated that the distribution is mainly skewed right. This means that there is an increase in development of new fine cracks with most of the existing crack widths remaining constant.

For the sustained tensile loading specimens the average crack width was found to be smaller than 300 µm with the exception of one specimen loaded at 40 % of the ultimate tensile stress and which had an average crack width of larger than 300 µm. The average crack width over time for each test specimen is shown to be a function of the number of cracks that develop and the sustained load applied. The same observation is made in terms of the number of cracks that form under a sustained load, as was observed for the quasi-static tensile tests. The number of cracks stabilises, after which the cracks widen, followed by eventual significant widening and failure at a single crack or multiple cracks. The developed crack widths at higher stress levels are primarily described with a skewed right distribution. However, at lower stress levels the distribution of the crack widths can be

represented by a normal distribution. The number of cracks that develop at low sustained tensile loads is much lower than at the higher sustained loads. This is a concern, since there is less cracks forming and wider cracks at low sustained loads.

The number of cracks that develop under a sustained load is significantly lower than what is observed for the rate tests at the same average strain level. The crack distribution in terms of the crack widths for the uni-axial quasi-static and sustained tensile loading tests can not be described by a normal distribution and is best represented by a skewed distribution with the exception at lower sustained tensile loads. Therefore, the statistical property, namely the skewness is of importance for the quantification of the distribution of the crack widths. When looking at different types of tensile tests the loading has a significant effect on the skewness of the distribution of the crack widths which is an indication of different failure mechanisms in terms of the number of cracks that develop or the significant increase in the average crack width.

6.2 Future Developments

The future development of SHCC is important to be able to use this advanced concrete material efficiently and for the correct purpose. The work presented in this thesis gave rise to numerous points that must be considered in the future and are summarised as follows:

- The investigation on the non-uniform cracking behaviour over the width of the test specimens needs attention. The use of multiple lines, as opposed to a single centre line as described in Chapter 3 may be more representative of the cracking behaviour over the width of the specimen. The fibre orientation as well as the support conditions has a crucial effect on the cracking behaviour.

- The age at testing needs to be investigated to determine what the cracking behaviour is at and beyond 28 days. The use of fly ash in the composite makes the hydration process slower which in turn decreases the strength of the fibre/matrix interface.

This could have a significant effect on the cracking behaviour and could lead to smaller crack widths at higher age.

- The creep fracture limit as well as the reliability of this SHCC should be investigated as well as the linear and non-linear behaviour of this material under a sustained load. The effect of the size of the specimen could be incorporated into this study. The use of thicker specimens, namely 30 mm x 30 mm to test the structural application of this material.

- The crack velocity for the quasi-static and creep specimens should be investigated to determine the crack growth.

- The creep of the fibres needs to be investigated seeing that the fibres plays a significant role in the average crack width as indicated in Chapter 5.

- The use of a hybrid mixture in terms of fibre content, namely short fibres and longer fibres can be investigated for the time-dependant cracking behaviour.

CHAPTER 7

REFERENCES

Aveston, J., Cooper, G.A. and Kelly, A., 1971, "Single and multiple fracture in the properties of fiber Composites", Conf. Proc., NPL, IPC Science and Technology Press Ltd., pp. 15-24.

Bao, G. and Song, Y., 1993, "Crack bridging models for fibre composites with degraded interfaces", J. Mech. Phys. Solids, Elsevier Science Ltd, Vol. 41, pp. 1425-1444.

Boshoff, W.P., 2007, "Time-dependant behaviour of Engineered Cement-based Composites", PhD Dissertation, Stellenbosch University, South Africa.

Boshoff, W.P. and Van Zijl, G.P.A.G., 2007, "Time-dependant response of ECC: Characterisation of creep and rate dependence", Cement and Concrete Research, Elsevier, Vol 37, pp. 725-734.

Boshoff, W.P., Adendorff, C.J. and Van Zijl, G.P.A.G., 2008, "Creep of cracked strain hardening cement-based composites," Concreep8 Conference, Vol.1, Oct., pp.723-728.

British Standard EN 1015-3:1999, "Methods of test for mortar for masonry - Part 3: Determination of consistence of fresh mortar (by flow table)".

Bulmer, M.G., 1965, "Principles of Statistics", United States of America, New York.

JCI-DFRCC Committee, 2002, JCI-DFRCC summary report on DFRCC terminologies and application concepts, Proceedings of the JCI International Workshop on Ductile Fibre Reinforced Cementitious Composites (DFRCC) – Application and Evaluation (DFRCC-2002), Takayama, Japan, Oct. 2002, pp. 59-66.

Jun, P. and Mechtcherine, V., 2008, "Deformation behaviour of cracked Strain-Hardening Cement-based Composites (SHCC) under sustained and repeated tensile loading", Concreep8 Conference, Vol.1, Oct., pp.487-493.

Kamal, A., Kunieda, M., Ueda, N. and Nakamura, H., 2008, "Evaluation of crack opening performance of a repair material with strain hardening behavior", Cement & Concrete Composites 30, pp. 863–871.

Kanda, T. and Li, V.C., 1998, "Multiple Cracking Sequence and Saturation in Fiber Reinforced Cementitious Composites", Concrete Research and Technology, Vol. 9, No2.

Kim, D.J., El-Tawil, S. and Naaman, A.E., 2008, "Rate-dependant tensile behavior of high performance fiber reinforced cementitious composites", RILEM.

Krencher, H., and Stang, H., 1988, "Stable Microcracking in Cementitious Materials", Proceedings of 2nd International Symposium on Brittle Matrix Composites, pp. 20-33.

Lepech, M.D. and Li, V.C., 2005, "Water permeability of cracked cementitious composites", Proceeding of ICF, Torino.

Li, V.C., 1992, "Performance driven design of fiber reinforced cementitious composites", Published by E & FN Spon, London, ISBN 0 419 18130 X.

Li, V.C., 1993, "From micromechanics to structural engineering – The design of cementitious composites for civil engineering applications", Japan Society of Civil Engineers, Japan, Vol. 10 pp 37-48.

Li, V.C., 1998, "Engineered Cementitious Composites - Tailored Composites through Micromechanical Modeling in Fiber Reinforced Concrete: Present and the Future", edited by N. Banthia, A. Bentur, A. and A. Mufti, Canadian Society for Civil Engineering, Montreal, pp. 64-97.

Li, V.C., 2002, "Reflections on the research and development of engineered cementitious composites", Proceeding of ICF, Torino.

Li, V.C. and Chan, Y.W., 1993, "Determination of interfacial debonding mode for fibre reinforced cementitious composites", ACS, Japan.

Li, V.C., Wang, S. and Wu, C., 2001, "Tensile Strain-hardening Behavior of PVAECC," ACI Materials Journal, Vol. 98, No. 6, pp 483-492.

Lin, Z. and Li, V.C., 1997, "Crack bridging in Fiber Reinforced Cementitious Composites with slip-hardening interfaces," J. Mech. Phys. Solids, Elsevier Science Ltd, Vol. 45, No. 5, pp. 763-787.

Lin, Z., Kanda, T. and Li, V.C., 1999, "On Interface Property Characterization and Performance of Fiber Reinforced Cementitious Composites," J. Concrete Science and Engineering, RILEM, Vol. 1, pp. 173-184.

Maalej, M., and Li, V.C., 1996, "Introduction of Strain-Hardening Engineered Cementitious Composites in Design of Reinforced Concrete Flexural Members for Improved Durability", ACI Structural Journal, Vol. 92, No. 2.

Moriyama, M., Morii, N., Itagaki, K. and Rokugo, K., 2009, "Multi-layer spray lining using multiple fine cracking type fibre reinforced cementitious composites (HPFRCC)," 4th International Conference on construction materials: Performance, Innovations and Structural Implications, Vol 1, pp. 419 – 425.

Redon, C., Li, V.C., Wu, C., Hoshiro, H., Saito, T. and Ogawa, A., 2001, "Measuring and Modifying Interface properties of PVA Fibers in ECC Matrix," ASCE J. Materials in Civil Engineering, Vol. 13, No. 6, pp 399-406.

Robins, P., Austin, S., Chandler, J. and Jones, P., 2001, "Flexural strain and crack width measurement of steel-fibre-reinforced concrete by optical grid and electrical gauge methods," Cement and Concrete Research, Vol. 31, pp 719-729.

Rouse, J.M. and Billington, S.L., 2007, "Creep and Shrinkage of High-Performance Fiber-Reinforced Cementitious Composites," ACI Materials Journal, V. 104, No. 2, March-April.

Rüsch, H, 1960, "Research toward a general flexural theory for structural concrete," ACI Journal, Vol. 57.

Weimann, M.B. and Li, V.C., 2003, "Drying Shrinkage and Crack Width of ECC", BMC-7, Poland, pp. 37-46.

Wu, H.C. and Li, V.C., 1995, "Stochastic process of multiple cracking in discontinuous random fibre reinforced Brittle Matrix Composites", International Journal of damage mechanics, Vol 4, No 1, pp. 83 – 102.

Zhou, F.P., 1992, "Time-dependant Crack Growth and Fracture in Concrete," Dissertation, Lund University, Lund, Sweden.